Desalination and Water Treatment
www.deswater.com
doi: 10.5004/dwt.2019.24758

171 (2019) 223–249
December

Adsorption performances of branched aminated waste polyacrylonitrile fibers: experimental versus modelling study

Krstimir Pantić[a], Zoran J. Bajić[b,*], Zlate S. Veličković[b], Veljko R. Djokić[a], Jelena D. Rusmirović[c], Aleksandar D. Marinković[a], Aleksandra Perić-Grujić[a]

[a]*University of Belgrade, Faculty of Technology and Metallurgy, 4 Karnegijeva street, 11120 Belgrade, Serbia, emails: pantic_krstimir@yahoo.com (K. Pantić), djokicveljko@yahoo.com (V.R. Djokić), marinko@tmf.bg.ac.rs (A.D. Marinković), alexp@tmf.bg.ac.rs (A. Perić-Grujić)*
[b]*Military Academy, University of Defense, 33 General Pavle Jurišić – Šturm street, 11000 Belgrade, Serbia, emails: zoran.bajic@va.mod.gov.rs (Z.J. Bajić), zlatevel@yahoo.com (Z.S. Veličković)*
[c]*Innovation Center of the Faculty of Technology and Metallurgy Ltd., 4 Karnegijeva street, 11120 Belgrade, Serbia, email: jrusmirovic@tmf.bg.ac.rs*

Received 12 March 2019; Accepted 31 July 019

ABSTRACT

Synthesis of branched aminated waste polyacrylonitrile (PAN) fibers, realized in a three addition/amidation successive steps, was performed in order to obtain AS3-PAN adsorbent. Influence of various operating parameters such as pH, contact time, adsorbent mass and initial concentration of pollutants, on adsorption capacity has been studied. Design of the experimental plan of adsorption experiments, defined by response surface methodology (RSM), rationalized the number of necessary experiments. The calculated adsorption capacities for AS3-PAN, obtained by Langmuir model, were 58.94, 41.07, 34.51, 24.54 and 29.61 mg g^{-1} for Pb^{2+}, Cd^{2+}, Ni^{2+}, Cr(VI) and As(V) ion, respectively. The results of pseudo-second-order reaction rate and Weber-Morris kinetic model indicated significant resistance due to intra-particle (pore) diffusion. The experimental results were compared with the theoretically calculated ones, obtained by RSM prediction model, and validation of applied methodology was performed by testing the quality of the regression analysis with analysis of variance test.

Keywords: PAN adsorbent; Amino terminated PAN; RSM method; Adsorption models; Heavy metals

1. Introduction

Environmental pollution, caused by releasing of toxic compounds from industries, such as heavy metal ions (lead, cadmium, nickel) and oxyions (chromium and arsenic), has attracted much concern in recent years [1]. These heavy metal ionic forms are classified amongst the omnipresent toxic and carcinogen metal elements linked to numerous forms of skin, lung, liver, bladder, and kidney cancers [2]. Moreover, their toxic effect is caused by replacing divalent metal ions contained naturally in biological systems (calcium, zinc, magnesium etc.) followed with modification of active biological molecule conformations and blocking of essential functional groups [3]. Heavy metals mainly originate from industrial activities and geochemical processes, and due to their high stability, they represent great pollution problem. According to the World Health Organization recommendations, maximum allowable content of heavy metal ions/oxyanions in drinking water was defined to be lower than 0.005 mg L^{-1} [3].

Therefore, it is important to develop a highly efficient, reliable and economically cost-effective technique for heavy metal ion/oxyanion removal from natural and wastewaters. Various treatment methods such as ultrafiltration, ion

* Corresponding author.

exchange, coagulation/precipitation, membrane filtration, reverse osmosis, and adsorption have been used for wastewater purification [4–6]. Among the above technologies, adsorption is classified as promising technology due to its simplicity in design, ease of handling and ability to overcome secondary pollutants [7].

Many adsorbents have been reported in the literature for the removal of heavy metal ions/oxyanions such as amino-modified nanocellulose impregnated with iron oxide [8], amino modified and oxidized multi-walled carbon nanotubes [9], hydrolyzed polyacrylonitrile (PAN) fibers [10], hyperbranched polyethylenimine functionalized PAN fibers [11], thiosemicarbazide modified PAN fibers [12], phosphinic acid functionalized PAN fibers [13] and iron-oxide-coated eggshell and porous wollastonite as natural based adsorbents [14]. Among them, PAN fibers are one of the most promising fibers because of its low-cost, large surface areas suitable for functionalization and improved mechanical properties and easily application in flow processes conditioned by woven into various shapes [15]. From the practical application point, the PAN based absorbents possess much desirable superiority in solvent resistance, thermal and mechanical stability [12]. To activate a tight binding of PAN fibers with metal ions/oxyions, the grafting of various functional moieties containing nitrogen is important [11]. The introduction of amino group by surface functionalization is well known method used to improve adsorption capability/affinity of numerous fibers like materials towards metal ions. In that way, the amino modified PAN based adsorbent is especially convenient because it considerably improves the adsorbent susceptibility for heavy metal ions from aqueous solutions.

Besides the design of adsorbent surface, related to the adsorbent/pollutant interaction, it is also important to perform the actual study of the adsorbent characteristics. Never the less, the information on its applicability in real systems includes hundreds of adsorption experiments combining different variable factors (adsorbent mass, initial solution concentration, pH value of the solution, adsorption temperature and time). In some recent studies, different methods of modelling and optimization, in order to predict the results and reduce the adsorption experiment number, were used. Response surface methodology (RSM), adaptive neural networks (neuro-fuzzy networks), modelling using a system of nonlinear algebraic and partial differential equations and discrete empirical interpolation method were used more frequently than the others [16]. These statistical optimization tools analyze system performance in order to assess the impact of the variation of selected variables.

RSM methodology has already been used in the optimization of the synthesis of adsorbents [8,17], the optimization of adsorption experiments [18,19] but the comparison of the results obtained by the RSM prediction model to the experimentally obtained results has not been done up till now. The commercial software Design Expert 9.0 with its statistical and graphical tools has been used in this study. Applied software provides complete comfort in the design of appropriate experiments, that is, the prediction of the results depending on the variables and validating the results obtained by examining the regression using analysis of variance (ANOVA) test. The use of RSM method makes possible to decrease the number of necessary experimental data associated with new processes, that is, optimization of adsorbent synthesis, and prediction of adsorption results. The strength of the method lies in possibility of obtaining accurate predictions of experimental results on the basis of accurate data that are collected from numerical or practical experiments at discrete data points in the design space. RSM design based on the multivariate approach enables substantial improvement/efficiency in the method development using lower number of necessary experiments. Moreover, it also causes using of small materials and solvents quantity and decreasing the time necessary to obtain satisfactory results.

In this study, waste PAN based adsorbent was synthesized by three-step surface modification: amination with diethylenetriamine (DETA) (AS1-PAN), structure branching by reacting with ethylenediamine tetraacetic ethyl ester (EDTA ester) (AS2-PAN) and amidation with DETA to provide large number of amino groups on AS3-PAN surface. Adsorption properties of AS3-PAN in a process of Cd^{2+}, Pb^{2+} and Ni^{2+} cation and Cr(VI) and As(V) oxyanion removal from water was examined. Specific objectives of this study were focused on: (i) preparation of hipper branched amino terminated waste PAN based adsorbent, (ii) adsorbent structural and morphological characterization, (iii) application of five level Central Composite experimental design combining with RSM to optimize the various parameters in order to obtain maximum adsorptive response, (iv) validation of the model and operational conditions optimization, (v) modeling of adsorption process using different isotherm and kinetic models, and (vi) comparison of modeling data and experimental ones in order to evaluate the applied methodology. The use of RSM to design of adsorption experiments was aimed to reduce the expensive and time-consuming experimental work and analysis, as well as to test possibility to predict adsorption data based on limited number of experimentally obtained ones.

2. Experimental part

2.1. Materials and chemicals

Material used for modification was waste PAN fibers (acrylonitrile monomer 91.7% and methyl acrylate comonomer 8.3%, according to the manufacturer specifications) was obtained from the carpet factory "Sintelon" Serbia. All chemicals and reagents were used as received: DETA, (Ducksan chemicals, BanWol Industrial Complex 608B-2L, 635-1 Seonggok-dong, Ansan-si, Gyeonggi-do, South Korea); Ethylenediamine tetraacetic acid anhydrous (EDTA), (Sigma-Aldrich Chemie GmbH Eschenstrasse 5 D-82024 Taufkirchen, Deutschland, p.a.); N,N′-Dicyclohexylcarbodiimide (DCC), (Sigma-Aldrich, p.a.); Trichloromethane (THM), $CHCl_3$, (Sigma-Aldrich, p.a.); Dichloromethane (DCM), (Sigma-Aldrich, p.a.); N,N-dimethylformamide (DMF); Concentrated hydrochloric acid (HCl); Sodium hydroxide (NaOH); Sodium hydrogen carbonate ($NaHCO_3$) Concentrated nitric acid, HNO_3, (Honeywell Fluka, (Seelze, Germany), ultra pure); Acetone (Sigma-Aldrich, p.a.); Absolute ethanol (Sigma-Aldrich, p.a.); Methanol (Sigma-Aldrich, p.a.); Deionized water (DW), that is. Milli-Q (Integral Water Purification System for Ultrapure Water, Merck KGaA, Darmstadt,

Germany) water (DW) with 18 MΩ resistivity was used. The lead, nickel, cadmium, arsenic and chromium standard solutions (Sigma-Aldrich), 1,000 mg L^{-1}, were further diluted with DW to the required concentration.

2.2. Adsorbent synthesis

Three successive synthesis steps were used in a production of PAN adsorbents:

2.2.1. Synthesis of DETA modified PAN fibers (AS1-PAN)

Waste PAN fibers (10 g) were rinsed with 100 mL of dichloromethane, treated with 100 mL N,N-dimethylformamide (DMF) at 40°C for 10 min, and washed with 50 mL of DW. Then, hydrolysis carried out in a 200 mL of ethanol/water solution (50/50 vol.) containing 2% (w/w) NaOH, was applied to attain appropriate extent of nitrile/ester groups hydrolysis; the solution was stirred at 45°C for 20 min; rinsed with 500 mL of DW, and dried for 6 h in the vacuum oven at 60°C. Dried hydrolyzed PAN fibers (10 g) were put in the Erlenmeyer flask filled with solution of 200 mL DETA and 400 mL DW. Fiber suspension was heated in the bath with reflux at 80°C for 10 h. After cooling to room temperature, obtained DETA functionalized PAN fibers (AS1-PAN) were filtered and washed with 200 mL of acetone/methanol, and then with 500 mL DW. Adsorbent AS1-PAN was dried in vacuum oven at 40°C for 6 h (Step I).

2.2.2. Modification of AS1-PAN with tetraethyl ester of EDTA (AS2-PAN)

In the dispersion of 10.28 g of the AS1-PAN in 100 mL of absolute ethanol, ethanol solution of tetraethyl2,2′,2′′,2′′′-(ethane-1,2-diylbis(azanediyl))tetraacetate (tetraethyl ester of EDTA) (27 g/100 mL) was added slowly. Tetraethyl ester of EDTA was prepared according to literature procedure [20]. Reaction took place at room temperature under ultrasonic treatment for 10 min, and followed with magnetic stirring for 6 h at 50°C. Product from Step II, denoted as AS2-PAN, was washed with ethanol, dried in a vacuum at 50°C for 6 h, and used in a subsequent step of modification, that is, Step III.

2.2.3. Modification of AS2-PAN with DETA (AS3-PAN)

AS2-PAN (11.32 g) was subjected to ultrasound treatment in 100 mL of dimethylformamide (DMF) for 5 min, dropwise addition of DETA (10 mL) for 10 min was followed by heating/mixing at magnetic stirrer for 5 h at 50°C. Obtained product was washed by using abundant quantity of DMF (200 mL), ethanol (300 mL) and DW (300 mL), dried at 60°C/12 h under vacuum (1,000 Pa), and denoted as AS3-PAN (mass 11.6 g). Schematic presentation of the procedure of PAN modification and the most probable structure/surface functionalities of synthesized adsorbents is presented in Fig. 1.

2.3. Methods used for the material characterization

Specific surface area (SSA), pore volume (PV), and pore size distribution were obtained from the nitrogen adsorption–desorption isotherm measured at 77.4 K using a Micrometrics Instrument Corporation (4356 Communications Drive, Norcross, GA 30093, USA) ASAP 2020 V1.05H surface area analyzer. The FTIR measurements were performed at room temperature in the transmission mode between 400 and 4,000 cm^{-1}, at resolution of 4 cm^{-1} using a Bomem Inc./Hartmann & Braun, (450 Saint-Jean-Baptiste Ave. Quebec, Canada) spectrometer. Scanning electron microscopy (SEM) was performed with a field emission scanning electron microscopy and electronic microscope SUPRA 35 VP (Carl Zeiss, Germany).

The pH values at the point of zero charge (pH_{PZC}), that is, the pH above which the total surface of the samples is negatively charged, of the samples were measured using the pH drift method [21]. A laboratory pH meter, Mettler Toledo FE20/FG2 (Switzerland), with the accuracy of ±0.01, was used for pH measurements. Ester value determination was performed according to standard ASTM D1617-07 [22]. Amino groups have essential influence on adsorption properties of amino modified PAN based adsorbent; therefore,

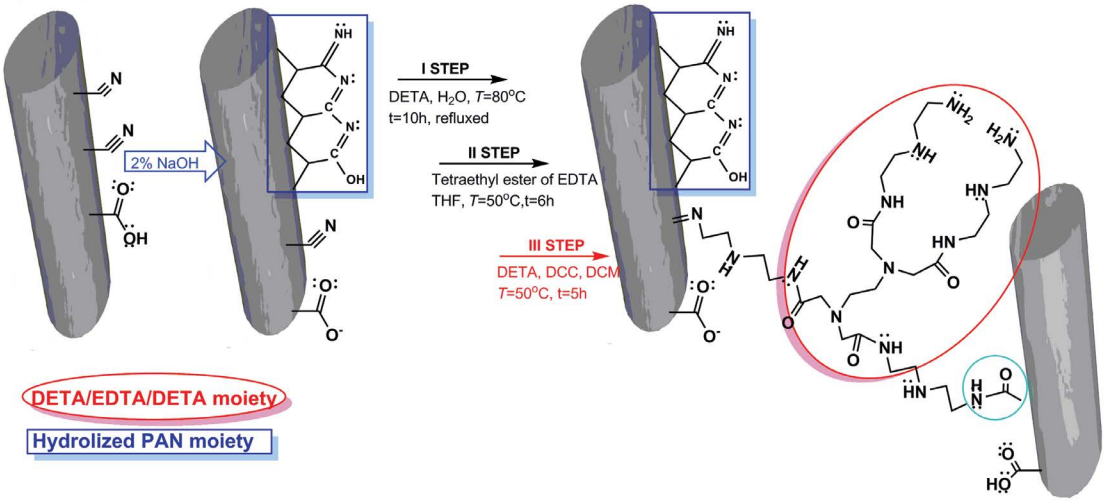

Fig. 1. Schematic presentation of chemical modification of waste PAN fibers.

it is very important to determine the conversion degree of nitrile groups into amino groups ($\Delta\omega$). $\Delta\omega$ is gravimetrically determined according to Eqs. (S1) and (S2).

Amino group content (AN) is determined via "back" (indirect) titration. 10 mg of PAN based adsorbent is placed in 20 mL 0.01 mol L^{-1} HCl and ultrasonicated for 30 min. Fibers are then filtered, and 10 mL of supernatant is titrated with standard solution of 0.01 mol L^{-1} NaOH in the presence of phenolphthalein. Aforementioned technique is based on the reaction of reactant with unknown concentration (amino group) and reactant in surplus with known concentration (HCl, 0.01 mol L^{-1}). The amount of excess HCl is determined with NaOH titration. The amount of amino group that reacted with HCl is determined based on difference of total amount of HCl used to treat AS3-PAN (20 mL) and the amount of HCl determined with NaOH titration. The acid value (AV) was determined using a standard method ASTM D3644 [23].

The content of ions before and after adsorption was determined by mass spectrometry with inductively coupled plasma (ICP-MS) using Agilent Technologies 7500ce ICP-MS system (Agilent Technologies, Inc., 5301 Stevens Creek Blvd. Santa Clara, CA 95051, United States).

All solutions were diluted and filtered through Millex-GV membrane filters of 0.22 μm pore diameter and analyzed on Dionex DX-300 ion chromatograph at 25°C. The device is equipped with Dionex IonPac AS 14 and Dionex IonPac AS 12 columns for analysis of anion and cation, respectively.

2.4. Batch adsorption experiment

Solutions of Cd^{2+}, Pb^{2+}, Ni^{2+}, As(V) and Cr(VI) ions with initial concentrations of $C_i[_{Cd}{}^{2+}]$: 0.096; 0.192; 0.481; 0.963; 1.923; 4.82 and 9.63 mg L^{-1}, $C_i[_{Pb}{}^{2+}]$: 0.102; 0.205; 0.512; 0.963; 2.56; 5.12 and 10.24 mg L^{-1} and $C_i[_{Ni}{}^{2+}]$: 0.101; 0.201; 0.505; 1.01; 2.52; 5.04 and 10.08 mg L^{-1}, $C_{i[As(V)]}$: 0.102; 0.204; 0.510; 1.020; 2.040; 5.10 and 10.20 mg L^{-1} and $C_{i[Cr(VI)]}$: 0.100; 0.200; 0.502; 1.004; 2.510; 5.029 and 10.04 mg L^{-1} were used in the batch experiments. In order to investigate the influence of pH values on the adsorption efficiency, initial pH (pH_i) was varied between 3.0 and 10.0. Thermodynamic and kinetic experiments were performed at 25°C, 35°C and 45°C. The influence of reaction time on the Cd^{2+}, Pb^{2+}, Ni^{2+}, Cr(VI) and As(V) ions adsorption was monitored in the interval at initial to 24 h. The amount of the adsorbed ions was calculated from the difference between the initial and equilibrium concentration. Furthermore, the influence of the ultrasound on the adsorption process during the stirring of the adsorbent-adsorbate solution was investigated in the preliminary trials in order to compare it to classic stirring methods. The results were analyzed using normalized standard deviation, Δq (%), calculated using Eq. (S3). The adsorption experiments were performed in triplicate and only mean values were reported. Maximum deviation is <4% (experimental error).

2.5. Design of adsorption experiments using RSM methodology

Prediction of adsorption results of Cd^{2+} ions in a batch system RSM was performed according to the presented research plan (Tables S1 and S2). Before starting an optimization procedure, it was of utmost importance to make selection of the crucial factors which affect the quality of the obtained modeling results. The levels for the variables were chosen on the basis of their minimum and maximum effect on capacity, and also each level has been tested at lower and higher end. RSM model was based on five-level-three-factor central rotatable composite design. Each experiment (except the central point) was performed in duplicate. The output variable was the adsorption capacity. The development of response surface models is an iterative process, and goodness-of-fit of any approximate model defines if the equation is satisfactory. Data obtained in these experiments were fitted with a second-order polynomial equation and the coefficients of the response function and their statistical significance were evaluated by the least squares method using commercial software Design-Expert, Software Version 9 (Stat-Ease, Inc. 2021 E. Hennepin. Suite 480 Minneapolis, USA). The Fisher test was used to determine the adequacy of the model and the Student's distribution to evaluate the significance of the coefficients. Analogous methodology was applied for Pb^{2+}, Ni^{2+}, Cr(VI) and As(V) ions.

3. Results and discussion

3.1. Adsorbent characterization

3.1.1. FTIR analysis

Characteristic absorption peaks of the AS3-PAN adsorbent, before and after pollutant adsorption, are presented in Table 1, while corresponding FTIR spectra are shown in Fig. S1. High intensity peak at 3,351 cm^{-1} corresponds to the stretching vibrations of NH_2/NH groups that is overlapped with OH group stretching vibrations, observed at 3,528 cm^{-1}, can be seen in the FTIR spectra of AS3-PAN adsorbent (Table 1, Fig. S1). Moderate peak at 2,938 cm^{-1} relates to the stretching vibrations of CH_2 and CH_3 groups (Table 1), while peak at 1,637 cm^{-1} is assigned to the stretching vibration of C=O group (amide band I, Table 1). Presence of unreacted nitrile groups, observed as the strong band positioned at 2,242 cm^{-1}, are found. Intense peak at 1,456 cm^{-1} corresponds to the deformation vibrations of methylene groups [24,25].

FTIR spectral data of coordination/complexes, AS3-PAN/Pb^{2+}, AS3-PAN/Cd^{2+} AS3-PAN/Ni^{2+}, AS3-PAN/Cr(VI) and AS3-PAN/As(V), given in Fig. S1 and Table 1, are compared with FTIR spectra of AS3-PAN before the adsorption. It has been shown that adsorption bands shift and peak intensities increase/decrease corresponding to the newly created amino/metallic complexes that include C=O, NH, CN and NH_2 groups (Fig. S1 and Table 1). Observable difference in the region of N–H stretching vibrations of hydroxyl, and primary and secondary amino groups (3,000–3,650 cm^{-1}) was noticed. Significant overlapping in this region is a result of hydrogen bonding interactions and cation/amine bonding types interactions causing change of bond force, that is, change of absorption band position. Low shifts can be noticed for C=O stretching vibration (ester and amide I), N–H deformation vibration coupled with n(C–N) vibration (amide II, ~1,580 cm^{-1}), C–N and C–H groups due to vibrations of different bonds from functionalized fibers in polymer-metal complex, as it is shown in Table 1. Overlapped bands at ~1,640 and ~1,585 cm^{-1} are assigned to a carbonyl amide stretching vibration (amide I) and N–H in-plane vibration, respectively, and after cation adsorption they shifted to higher wavelength. Also, bands at ~1,190 and ~820 cm^{-1}, which correspond to C–N stretching and out-of-plane NH_2

Table 1
FTIR analysis results of the AS3-PAN adsorbent before and after Cd^{2+}, Pb^{2+}, Ni^{2+}, Cr(VI) and As(V) ions adsorption

Bond	Wave number (cm^{-1}) of the group vibration in AS3-PAN/ion					
	AS3-PAN	Pb^{2+}	Cd^{2+}	Ni^{2+}	Cr(VI)	As(V)
N–H	3,528; 3,351	3,350	3,350	3,367	3,343	3,347
C–H	2,938	2,934	2,934	2,935	2,935	2,937
C=O (ester)	1,732	1,730	1,730	1,735	1,731	1,730
C=O (amide I)[a]	1,637	1,635	1,635	1,642	1,642	1,641
C–N	1,292	1,297	1,295	1,295	1,295	1,294; 798
C–O	1,051; 1,190	1,048; 1,187	1,045; 1,185	1,045; 1,185	1,049; 1,184	1,047; 1,185
M–O[b]	–	–	–	–	783	619
M=O[b]	–	–	–	–	905	523

[a]Amide band II are observed at ~1,580 cm^{-1}.
[b]Pb^{2+}, Cd^{2+}, Ni^{2+}, Cr(VI) and As(V).

Table 2
Textural properties, amino group content (AN), acid value (AV) and ester value (EV) of studied adsorbents

Adsorbent	SSA[a] ($m^2\ g^{-1}$)	PV ($cm^3\ g^{-1}$)	APD (nm)	pH_{PZC}	AN mmol g^{-1}	EV[b]/AV[c] mmol g^{-1}
AS1-PAN	5.1	0.018	1.2	6.2	0.029	–
AS2-PAN	6.9	0.022	1.3	6.5	0.008	0.075[a]
AS3-PAN	8.4	0.029	1.3	6.9	0.138	0.011[b]

[a]SSA of PAN is 1.2 $m^2\ g^{-1}$.
[b]EV – ester value.
[c]AV – acid value.

bending mode (twisting), respectively, almost completely disappear due to complexation/interactions of ion/amino groups. This indicates that positive charge of Cd^{2+}, Pb^{2+} and Ni^{2+} cations affect electronic density change at amide and amino group. Therefore, specific donor/acceptor interactions of cations with amino groups, both primary and secondary, restrict/modify their vibration modes (stretching, bending in- and out-of-plane) as it is registered by appropriate band shift [24,26].

After Cr(VI) sorption, two new bands appear at 783 and 906 cm^{-1} was attributed to the Cr–O and Cr=O bonds from the adsorbed Cr(VI) species. It suggests that Cr(VI) adsorption involve the amino functionalities on the AS3-PAN surface [24,27]. The presence of peaks at 618 and 523 cm^{-1} is due to the As–O and As=O bonding vibration which was observed after adsorption of As(V) [28].

FTIR of AS3-PAN could not indicate on degree of cross-linking, which is evidenced by low insolubility of AS3-PAN in DMF (negligible fraction; <5%) at reflux for 1 h. The samples obtained by reaction of PAN and DETA for the shorter time, less than 4 h, are completely soluble in DMF, which confirms relationship between modification efficiency versus reaction time and temperature [29]. This fact is of low importance to AS3-PAN adsorption performances, while it is interesting for consideration of future modification with long chain polyamine to achieve higher cross-linking degree useful in a production of a membrane type of adsorptive material.

3.1.2. Textural properties, pH_{PZC} and extent of functionalization

The results of textural properties determination: the SSA, PV and average pore diameter (APD) of AS3-PAN are determined from nitrogen adsorption/desorption isotherms and presented in Table 2.

The SSA and PV increase from 5.1 to 8.4 $m^2\ g^{-1}$ and from 0.018 to 0.029 $cm^3\ g^{-1}$ from AS1-PAN to AS3-PAN, respectively.

Stepwise modification of PAN by DETA, in the course of AS1-PAN synthesis, introduced 0.029 mmol g^{-1} of amino group (AN value). Higher amount of amino groups on AS1-PAN show basic properties, and thus pH_{PZC} (6.16) is increased in a comparison to unmodified PAN (3.5). Washing of PAN with basic solution provides ester and partial nitrile group hydrolysis producing hydroxyl/carboxyl groups as potential binding sites for cations [10]. Moderate extent of AS1-PAN modification with EDTA ethyl ester was verified by 0.075 mmol g^{-1} of introduced ester groups (~86% conversion) in AS2-PAN. The theoretical number of ester groups in AS2-PAN should be 0.087 mmol g^{-1}, indicating lower efficiency of transformation due to steric interference of the voluminous tetraethyl ester of EDTA. This is evident by low intensity peak at ~1,730 cm^{-1} originating from carbonyl stretch vibration of ester bond AS3-PAN (Fig. S1). The increased number of total basic sites, 0.138 mmol g^{-1} for AS3-PAN contributes to higher adsorption efficiency. This has been also evidenced by mass increase of AS3-PAN fibers for approximately 12% after modification. Adsorbent surface property, defined by pH_{pzc}, reflects the neutral net charge at adsorbent surface. Increased number of amino groups contributes to increase of

pH_{PZC}, and thus highest value of pH_{PZC} of 6.9 was found for AS3-PAN (Table 2). Positive surface potential at $pH < pH_{PZC}$ is a consequence of the nitrogen basicity, that is, protonation of both $–NH_2$, primary, and –NH–, secondary, amino groups. Presented results indicate significance of pH selection to control and adjust adsorbent performances.

3.2. SEM analysis

The morphology and structure of PAN and AS3-PAN samples, studied using SEM microscopy, are analyzed from representative images shown in Fig. 2. These figures show that the smooth structure of PAN is altered due to the modification process, as it can be observed from Fig. 2b. Outer diameter of 10–12 μm can be noticed which is specified in the manufacturers' technical data. Modified AS3-PAN fibers are filled with occasional lumps with curvy trench like structure, mutually interrelated through defect spots (nanometer size irregularity). Similar morphology of AS3-PAN fibers was found after pollutant adsorption.

3.3. Influence of solution pH on adsorption efficiency

Effect of solution pH on the AS3-PAN adsorption efficiency is studied in the range from 3 to 10, and the obtained results are shown in Fig. 3. Adsorption capability of AS3-PAN relates to both pH dependent pollutant speciation and generated adsorbent surface charges. In order to eliminate influence of the precipitation of metal hydroxide at higher pH, theoretical calculation (obtained using MINTEQ 3.0 software given in Figs. S2 and S3, and Fig. 3) and experimental study were performed without addition of adsorbent [9]. Theoretical and experimental results showed that the precipitation of $Pb(OH)_2$ at pH > 8, $Ni(OH)_2$ at pH > 9.5 and $Cd(OH)_2$ at pH > 9 takes place (Fig. 3a), which contributes to the extent of adsorption in this pH region. Adsorption curves at pH > 7 (Fig. 3a), represent the difference between the total amount of initial metal and ones found in a precipitated metal hydroxide.

Noticeable extent of cations adsorption in the pH region from 6.5–9 can be observed from Fig. 3a. The cations speciation is shown in Fig. S2. The metal ions removal at pH lower than 5 is low due to protonation of amino group (electrostatic repulsion of ammonium group with Cd^{2+}, Pb^{2+} and Ni^{2+} ions) and competition of H^+/cation for the same adsorption sites [9]. The increase of pH causes deprotonation of ammonium group, and at pH 6.92 equal amounts of acidic and basic groups exist on AS3-PAN surface. Cations are strongly bonded to amino groups by creating complexes/chelate system and attractive electrostatic interaction. Higher nucleophilicity/basicity of amino groups, at pH higher than pH_{PZC}, serve as coordination sites for metal binding. The decrease of adsorption capacity at higher pH (Fig. 3), relates to the hydrolysis of metal cation and generation of ionic species with lower affinity with respect to amino groups, e.g. $M(OH)^+$ at pH > 7. To ensure maximum adsorption of Cd^{2+}, Pb^{2+} and Ni^{2+} ions, pH 8, 6 and 7 were selected, respectively. At optimal pH value, the 82%–87 %, 92%–97% and 66%–71% of Cd^{2+}, Pb^{2+} and Ni^{2+} ions removal were obtained, respectively.

On the other side, at $pH < pH_{PZC}$ positively charged AS3-PAN surface causes attraction with negatively charged oxyanion (Fig. S3). In that way, applicability of the AS3-PAN is dictated by initial pH solution: the adjustment of pH of inlet water influences adsorption efficiency of the AS3-PAN with respect to either oxyanions or cations. The degree of As(V) and Cr(VI) removal vs. initial pH in presence of

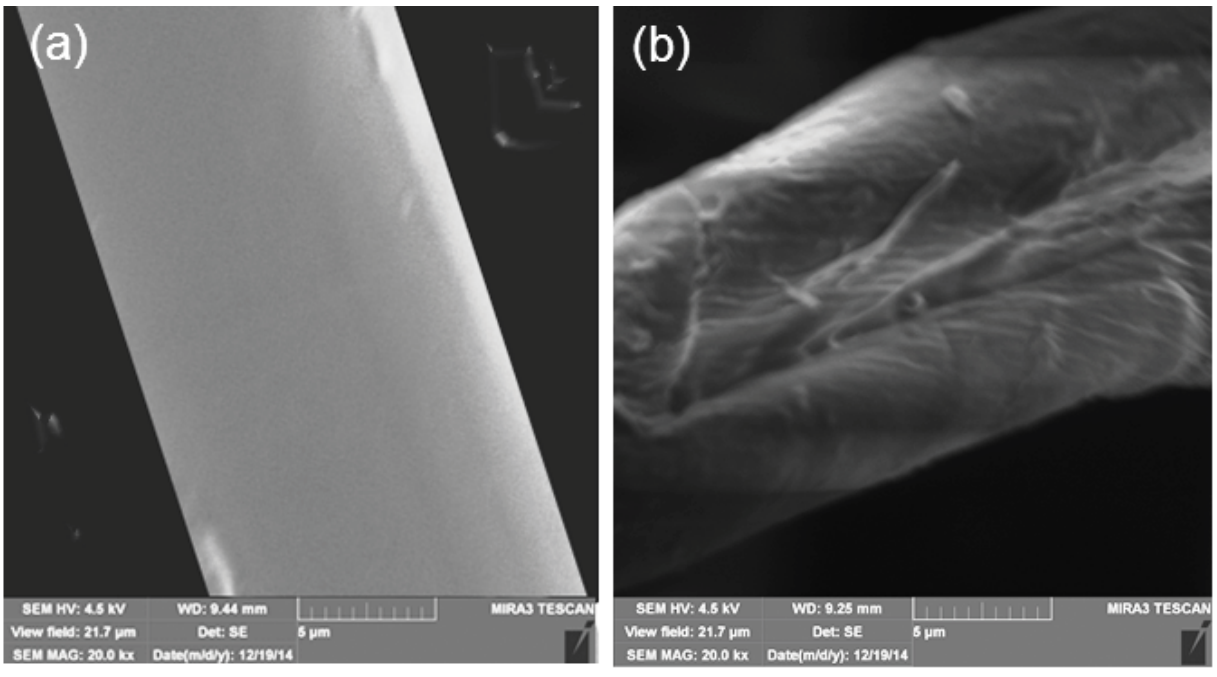

Fig. 2. SEM images of PAN fiber before (a) and after the three-step amino modification, that is, AS3-PAN adsorbent (b).

studied adsorbent is presented in Fig. 3b. It could be noted that As(V) adsorption on AS3-PAN is almost independent in the pH range 5–7 with >65% removal, and subsequently gradual decrease is observed at pH > 7. The pH-dependent successive ionization of triprotic arsenic acid (H_3AsO_4) could be presented by following equilibria:

$$H_3AsO_4 \xleftrightarrow{pKa(1)=2.3} H^+ + H_2AsO_4^- \xleftrightarrow{pKa(2)=7.0} 2H^+ + HAsO_4^{2-} \xleftrightarrow{pKa(3)=11.5} 3H^+ + AsO_4^{3-}$$

Presence of molecular form at pH < 2 and equilibrium of arsenate ionic forms at higher pH [26] plays crucial role in adsorption processes. Weak arsenic acid effectively interacts with AS3-PAN at pH in the vicinity of pKa. Similar consideration stands for chromic acid. At this condition the negatively charged As(V) species, that is, $H_2AsO_4^-$ and $HAsO_4^{2-}$ (Fig. S3), and Cr(VI) species, that's is, $HCrO_4^-$ and CrO_4^{2-} (Fig. S3), participate in an electrostatic attraction with positively charged adsorbent surface at pH < pH_{PZC}. Oppositely, at pH > pH_{PZC}, electrostatic repulsion is the main operative force, causing low adsorption efficiency. Accordingly, selection of pH 6 as initial pH value was dictated by three factors: adsorption capacity, adsorbent stability and accordance with pH of natural water used as inlet water in adsorption experiment (avoidance of pH adjustment on inlet water). Higher hydrolytic stability of surface functionalities, that is, long term adsorbent usability, in the pH range from 6.5 to 8 is a very important category from the techno-economical aspect.

3.4. Time-dependent adsorption study

The influence of the contact time is analyzed from the aspect of the most appropriate description/modeling of time-dependent adsorption data. The kinetic of pollutants removal from water is shown in Fig. 4. It can be noticed from Fig. 4 that the ultrasound treatment (Bandelin electronic, Berlin, Germany, power 120 W, frequency 35 kHz) contributes to fast achievement of adsorption equilibrium, almost 6–7 times faster (120 min) than the classical mixing with laboratory shaker (mixing speed of 120 rpm for 150 min).

The application of ultrasound field increases the adsorption rate as a consequence of mass transfer resistance decrease. Ultrasound waves and side effect of the bubble cavitation, near to adsorbent substance cause micro disturbances reducing boundary layer which, in the other hand, cause improvement of mass transfer. Ultrasound could modify mechanism of adsorption process but increase adsorption rate causing faster system equilibration [14]. It is also noticed that after 90 and 105 min of adsorption under ultrasound and classical mixing, efficiencies were almost constant (at >98% removal; Fig. 4). Due to low benefit ultrasound treatment was not considered in further experiments, and adsorption time was fixed to 120 min.

3.5. Adsorption kinetics

The obtained results, based on most commonly used kinetic adsorption models: Pseudo-first-order, Pseudo-second-order (PSO) and Second order [30], given by the Eqs. (S4)–(S6), adsorption capacity (q_e), rate constant (k) and linear regression coefficient (R^2), are shown in Table 3.

The best fitting was obtained using PSO equation which means that both the concentrations of adsorbate and adsorbent (AS3-PAN) are involved in the rate limiting step of the overall adsorption process [9,21]. The constants k (Table 3) refer fastest rate for Cd^{2+}, Pb^{2+} and lowest one of equilibrium attainment for As(V). The effect of ionic radii of the metal ions could not help in explaining the trend of kinetic results, but it should not be neglected that the charge of ion and the number of water molecules, their distribution/-coordination in solvation shell influence the diameter of the hydration layer, which, in turn plays particular role in ion mobility. Taking this aspect into account, both a lower radius of the hydration shell and a more labile bonding contribute to increased removal efficiency.

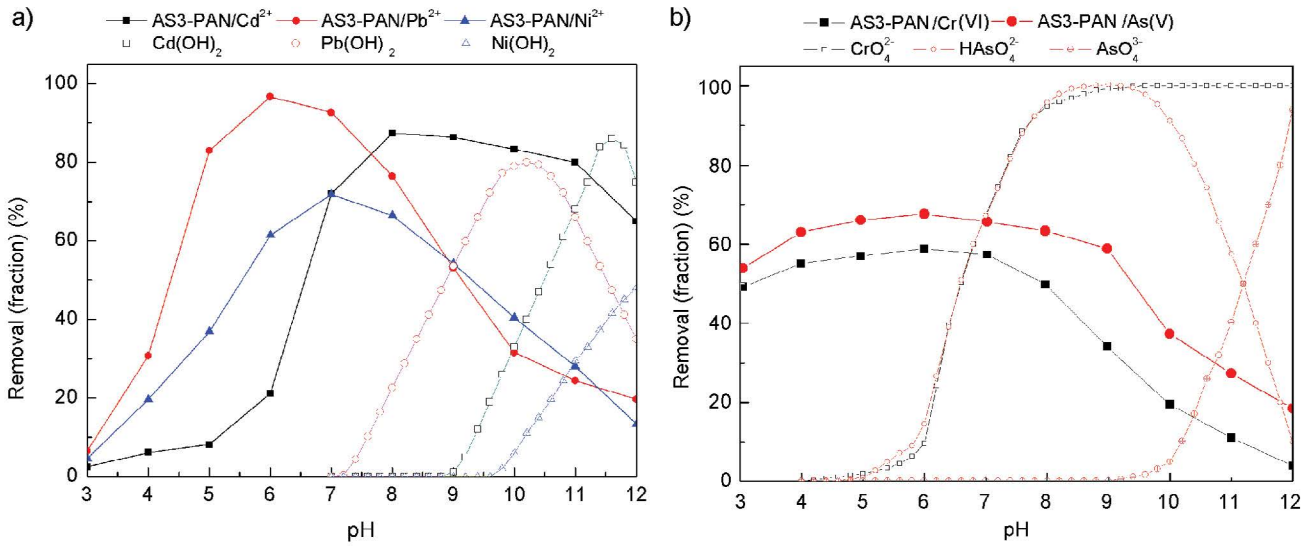

Fig. 3. Influence of pH on the adsorption of (a) Cd^{2+}, Pb^{2+} and Ni^{2+}, and (b) Cr(VI) and As(V) ions on AS3-PAN (in %) [$C_i[_{Cd}{}^{2+}]$ = 4.82 mg L^{-1}, $C_i[_{Pb}{}^{2+}]$ = 5.12 mg L^{-1}, $C_i[_{Ni}{}^{2+}]$ = 5.002 mg L^{-1}, $C_{i[Cr(VI)]}$ = 5.02 mg L^{-1}, $C_{i[As(V)]}$ = 5.1 mg L^{-1}, m/V = 200 mg L^{-1} and T = 25°C].

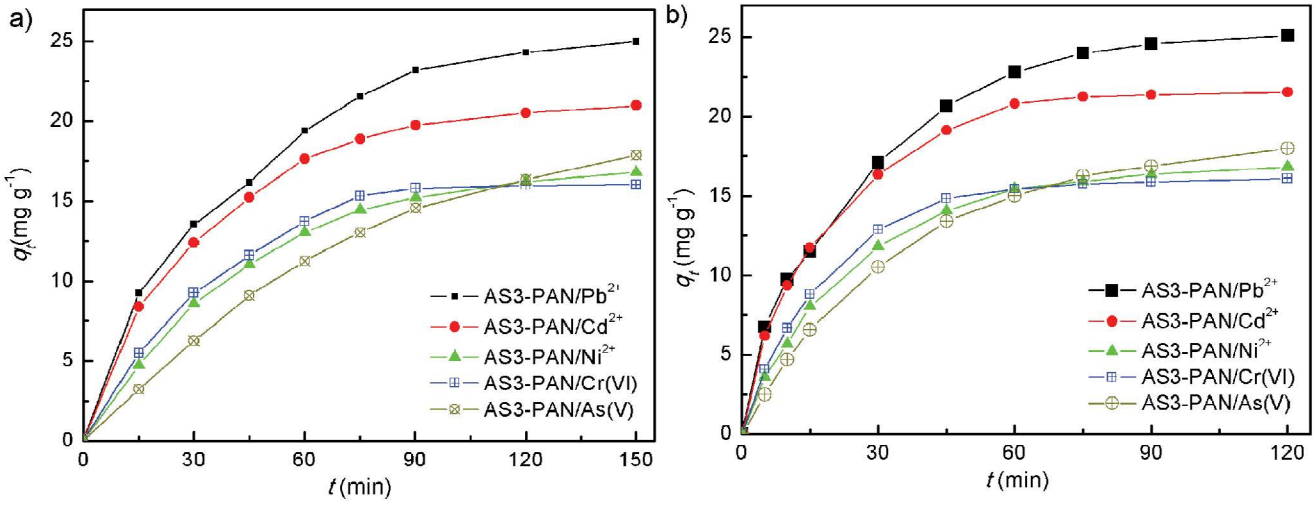

Fig. 4. Results of adsorption of Cd^{2+}, Pb^{2+}, Ni^{2+}, Cr(VI), and As(V) ions on AS3-PAN versus adsorption methods: (a) magnetic mixing and (b) ultrasound treatment [$C_i[_{Cd}{}^{2+}]$ = 4.82 mg L^{-1}, pH = 8; $C_i[_{Pb}{}^{2+}]$ = 5.12 mg L^{-1}, pH = 6; $C_i[_{Ni}{}^{2+}]$ = 5.002 mg L^{-1}, $C_{i[Cr(VI)]}$ = 5.02 mg L^{-1}, pH = 7, $C_{i[As(V)]}$ = 5.1 mg L^{-1}, pH = 6, m/V = 200 mg L^{-1} and T = 25°C].

Table 3
Kinetic parameters for AS3-PAN [$C_i[_{Cd}{}^{2+}]$ = 4.82 mg L^{-1}, pH = 8; $C_i[_{Pb}{}^{2+}]$ = 5.12 mg L^{-1}, pH = 6; $C_i[_{Ni}{}^{2+}]$ = 5.02 mg L^{-1}, $C_{i[Cr(VI)]}$ = 5.02 mg L^{-1}, pH = 7, $C_{i[As(V)]}$ = 5.1 mg L^{-1}, pH = 6, m/V = 200 mg L^{-1} and T = 25°C]

Sorbat/Order of kinetic law		Pseudo-first-order	Pseudo-second-order	Second-order
Cd^{2+}	q_e	6.258	21.586	20.224
	k (k_1, k_2)	0.0131	0.0223	0.0126
	R^2	0.748	0.998	0.784
Pb^{2+}	q_e	4.859	25.287	24.332
	k (k_1, k_2)	0.0372	0.0219	0.0653
	R^2	0.929	0.999	0.956
Ni^{2+}	q_e	12.096	16.957	15.835
	k (k_1, k_2)	0.0053	0.0160	0.0024
	R^2	0.902	0.999	0.935
Cr(VI)	q_e	13.744	16.251	15.242
	k (k_1, k_2)	0.0081	0.0167	0.0029
	R^2	0.666	0.998	0.702
As(V)	q_e	6.552	18.045	17.122
	k (k_1, k_2)	0.0124	0.0062	0.0034
	R^2	0.746	0.997	0.956

Moreover, owing to the limitation of PSO modeling in a description of the contribution of appropriate step in overall adsorbate transport (through the solution, surface film/intra-particular diffusion and adsorption/desorption equilibrium at adsorbent surface), diffusion kinetic model was used. The kinetic data, fitted using Elovich, intra-particle Weber–Morris (W-M), Dunwald-Wagner (D-W), homogenous solid diffusion (HSDM) model, were useful in evaluation of rate limiting step of overall process [17]. The obtained results are given in Table 4.

According to the results of W-M plot from Table 4, two linear relations with significant intercepts, higher for cation and lower for anions, were observed. High value of W-M constant C indicates that intra-particle diffusion is not the only rate-limiting step; influences of the other factors determine effectiveness of overall pollutant transport. At the initial stage of the process, the diffusion from bulk phase to the exterior surface takes place at high rate, while second and third linear part relate to the diffusion inside mesopores/micropores and adsorption/desorption processes. W-M plots of the kinetic data at different C_i gave similar pattern which means that higher ion flux does not affect multi-linearity, that is, change of adsorption mechanism and rate-limiting step (results not presented). Elovich equation showed good applicability in modeling dominantly chemisorption on heterogeneous adsorbents [31]. Even though the lower statistical validity of correlation using Elovich model (Table 4), the obtained results indicate that chemisorption could be a contributing factor

Table 4
Fitted kinetic data for the adsorption of Cd^{2+}, Pb^{2+}, Ni^{2+}, Cr(VI) and As(V) on AS3-PAN [$C_i[_{Cd}{}^{2+}]$ = 4.82 mg L^{-1}, pH = 8; $C_i[_{Pb}{}^{2+}]$ = 5.12 mg L^{-1}, pH = 6; $C_i[_{Ni}{}^{2+}]$ = 5.002 mg L^{-1}, $C_{i[Cr(VI)]}$ = 5.02 mg L^{-1}, pH = 7, $C_{i[As(V)]}$ = 5.1 mg L^{-1}, pH = 6, m/V = 200 mg L^{-1} and T = 25°C]

Kinetic model	Constants	Cd^{2+}	Pb^{2+}	Ni^{2+}	Cr(VI)	As(V)
Elovich	α (mg g^{-1} min^{-1})	13.054	5.394	21.729	20.613	5.564
	β (mg g^{-1})	0.517	0.161	0.393	0.382	0.291
	R^2	0.942	0.952	0.981	0.894	0.997
W-M (Step 1)	k_{p1} (mg g^{-1} $min^{-0.5}$)	1.365	1.325	1.418	2.512	1.713
	C (mg g^{-1})	12.939	16.736	8.400	3.245	3.872
	R^2	0.997	0.913	0.985	0.994	0.971
W-Ms (Step 2)	k_{p2} (mg g^{-1} $min^{-0.5}$)	0.0352	0.113	0.544	0.141	0.605
	C (mg g^{-1})	20.668	23.704	11.492	14.078	11.005
	R^2	0.979	0.978	0.955	0.999	0.999
D-W	K	0.0271	0.027	0.026	0.030	0.0213
	R^2	0.813	0.896	0.981	0.810	0.991
HSDM	$D_s \cdot 10^{11}$	2.89	2.93	2.84	3.36	2.56
	R^2	0.810	0.890	0.981	0.792	0.979

originating from high complexation ability of amino group toward cation. Apart from this, similar values of diffusion coefficients for cations, obtained by HSDM model, indicate their similar mobility, while higher diffusivity (D_s) for Cr(VI) is in a good accordance with somewhat higher value of rate constant in comparison to As(V) (Table 3). In the other hand, higher values of rate constants for cations reflect higher intensity interactions/affinity of amino group, comparing to dominant electrostatic interaction with oxyanion (Fig. 5).

3.6. Activation energy parameters

In order to determine kinetic activation parameters, determination of PSO rate constant was performed at 25°C, 35°C and 45°C. Values of q_e adsorption rate constant k, normalized standard deviation (Δq) and linear regression coefficient R^2 are presented in Table 5.

Obtained kinetic data at three different temperatures (Table 5), were used for calculation of activation parameters using linearized form of Arrhenius equation, given by Eq. (1):

$$\ln k_2 = -\frac{E_a}{RT} + \ln A \tag{1}$$

where k_2 is reaction rate constant, E_a denotes activation energy, R is universal gas constant (8.314), T is temperature in Kelvin, A is Arrhenius factor (frequency factor). Calculated E_a are as follows: 4.16, 4.89, 6.38, 5.53, 6.03 kJ mol^{-1} for Cd^{2+}, Pb^{2+}, Ni^{2+}, Cr(VI) and As(V) ions, respectively. The small difference between activation energies obtained points out to similar energetic requirement to overcome energetic barrier of the slowest adsorption step. Magnitudes of the activation energy can help in understanding the adsorption mechanism. Low values of E_a are in a close relation to low porosity of AS3-PAN (Table 2), or vice versa, diffusional processes do not control dominantly overall adsorption. Change of the rate controlling effect both diffusional processes and surface adsorption processes over time are also low, which is confirmed by change of mixing rate. According to literature data concerning relationship between activation energy and adsorption type, analyzed system indicates ton dominance of physisorption with participation of diffusion-controlled processes [32].

3.7. Competitive kinetic study

The evaluation of the rate of selective pollutant uptake is acquired from the competitive kinetic study. Obtained results offer valuable information for design of adsorbent with capability of selective pollutant removal from natural/polluted water. Results of competitive adsorption of Cd^{2+}, Pb^{2+} and Ni^{2+} in the presence of single interfering ion: Ca^{2+}, Al^{3+} and Fe^{3+} and multicomponent system (Ca^{2+}/Al^{3+}/Fe^{3+}), obtained by PSO fitting, are given in Table 6.

Single competitive Cd^{2+} removal (Table 6) shows the highest influence of the system of three cations (Ca^{2+}/Al^{3+}/Fe^{3+}) (66% lower k_2), followed by Al^{3+} (50%), Fe^{3+} (46%) and Ca^{2+} (18%). Similar trend of 72%, 44%, 43% and 15% of k_2 decrease, respectively, is obtained for Pb^{2+}. In addition, preliminary competitive kinetic study of As(V) and Cr(VI) uptake shows somewhat lower decreasing of rate constants in the presence of single interfering ion: SiO_4^{4-} or PO_4^{3-}. The highest decrease is obtained in presence of both anions and the decrease of k_2 is as follows: 32% for As(V) and 27% for Cr(VI) removal in presence of phosphate. Obtained results indicate low selectivity with respect to both cations and anions, which means that AS3-PAN could be effectively used as a general purpose adsorbent for preferential cations with simultaneous anion removal from multicomponent system.

3.8. Adsorption study

The state of interaction/bonding at solutes/sorbent surface at equilibrium is described by fitting experimental data with various adsorption isotherms [17,33]. Equilibrium

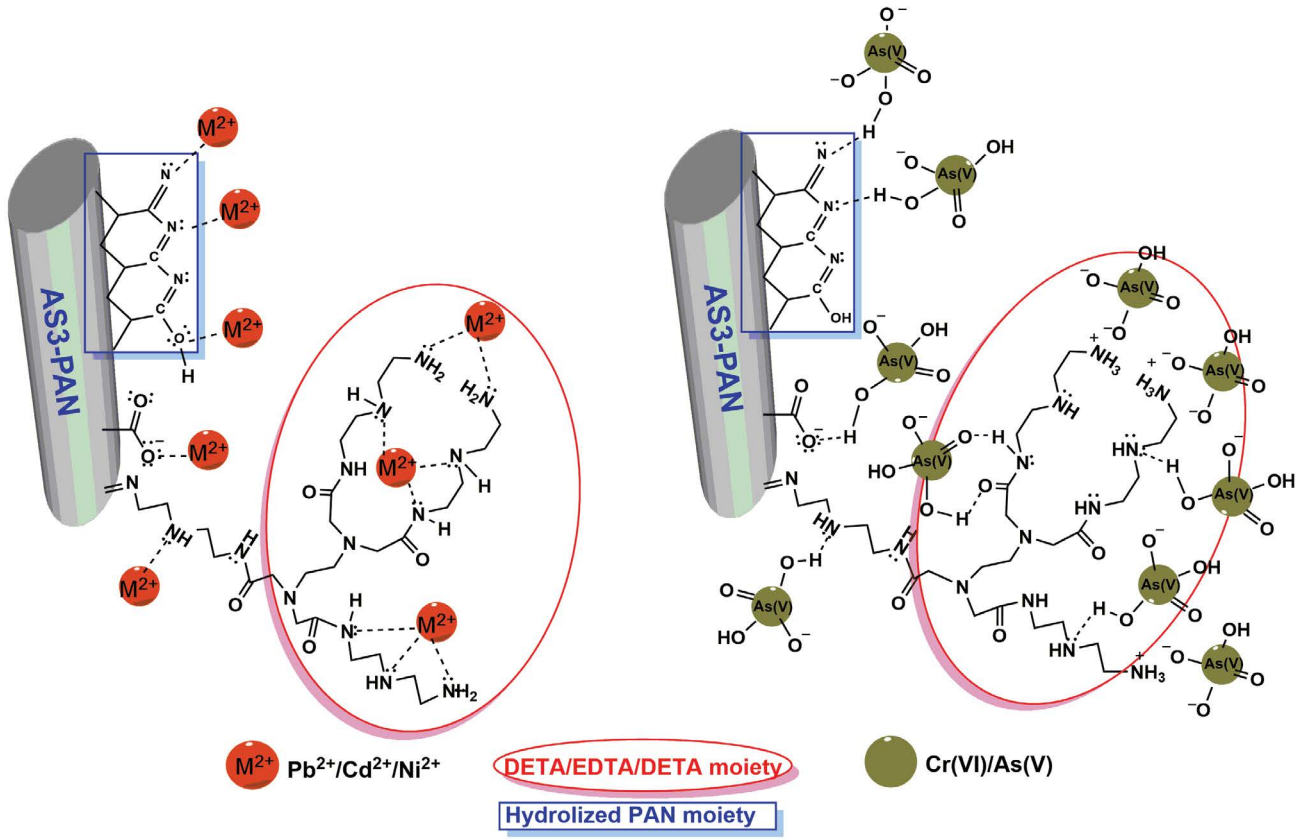

Fig. 5. Schematic presentation of bonding mechanism of cations (general mechanism) and oxyanions (example given for $H_2AsO_4^-/HAsO_4^{2-}$) with functionalities present on AS3-PAN surface.

Table 5
PSO model parameters for the adsorption of pollutants on AS3-PAN at 25°C, 35°C and 45°C temperature [$C_i[_{Cd}{}^{2+}]$ = 4.82 mg L^{-1}, pH = 8; $C_i[_{Pb}{}^{2+}]$ = 5.12 mg L^{-1}, pH = 6; $C_i[_{Ni}{}^{2+}]$ = 5.02 mg L^{-1}, pH = 7, $C_{i[Cr(VI)]}$ = 5.02 mg L^{-1}, pH = 7, $C_{i[As(V)]}$ = 5.1 mg L^{-1}, pH = 6, m/V = 200 mg L^{-1}]

	T	k_2 (g mg^{-1} min^{-1})	q_e (mg g^{-1})	Δq (%)	R^2
Cd^{2+}	25°C	0.02228	21.586	2.65	0.999
	35°C	0.02349	21.680	2.85	0.999
	45°C	0.02476	21.771	2.70	0.998
Pb^{2+}	25°C	0.02191	25.287	3.37	0.998
	35°C	0.02362	25.299	3.27	0.999
	45°C	0.02480	25.307	3.29	0.999
Ni^{2+}	25°C	0.01604	16.657	3.35	0.998
	35°C	0.01745	17.490	3.67	0.998
	45°C	0.01886	17.993	3.92	0.995
Cr(VI)	25°C	0.016764	16.252	3.15	0.994
	35°C	0.018277	16.905	3.28	0.991
	45°C	0.019791	17.659	3.10	0.999
As(V)	25°C	0.00617	18.044	3.70	0.999
	35°C	0.00668	18.428	3.54	0.999
	45°C	0.00719	18.619	3.85	0.989

adsorption data are best correlated using Langmuir (Eq. (S14)) or Freundlich (Eq. (S15)) isotherm model. Details on the main presumption incorporated in used isotherm models are given in Supplementary material.

Langmuir and Freundlich parameters (Figs. S4a and b), obtained by fitting the equilibrium adsorption data using isotherm models, are shown in Table 7. Higher values of R^2 for the Freundlich model indicate valid description of

Table 6
Results of the competitive Cd^{2+} and Pb^{2+} removal in the presence of interfering ions

Adsorbent	Parameters	Non-competitive condition	Competitive conditions			
			$Ca^{2+,a}$	$Al^{3+,a}$	$Fe^{3+,a}$	$Ca^{2+}/Al^{3+}/Fe^{3+,b}$
Cd^{2+}	q_e (mg g^{-1})	21.586	19.265	11.256	13.879	9.875
	k_2	0.0222	0.0182	0.0111	0.0120	0.0097
	R^2	0.999	0.996	0.996	0.997	0.995
Pb^{2+}	q_e (mg g^{-1})	25.287	23.459	14.854	15.966	9.568
	k_2	0.0219	0.0218	0.0143	0.0146	0.0071
	R^2	0.999	0.989	0.982	0.975	0.984

[a]Single competitive condition.
[b]System of three anion competition [$C_i[_{Cd}{}^{2+}]$ = 4.82 mg L^{-1}, pH = 8; $C_i[_{Pb}{}^{2+}]$ = 5.12 mg L^{-1}, pH = 6; m/V = 200 mg L^{-1}, T = 25°C]

Table 7
Langmuir and Freundlich isotherm parameters for pollutants removal using AS3-PAN

		Langmuir isotherm				Freundlich isotherm		
	T (°C)	q_{max} (mg g^{-1})	b (dm^3 mol^{-1})	b (L mg^{-1})	R^2	k_f (mol^{1-n} L^n g^{-1})	$1/n$	R^2
Cd^{2+}	25	38.98	412,754	3.672	0.948	22.84	0.493	0.993
	35	40.03	426,372	3.793	0.943	23.98	0.495	0.993
	45	41.07	442,549	3.937	0.937	25.03	0.496	0.992
Pb^{2+}	25	57.8	1,363,181	6.585	0.873	63.13	0.611	0.992
	35	58.51	1,430,546	6.911	0.869	66.56	0.614	0.991
	45	58.94	1,517,722	7.332	0.873	70.13	0.617	0.989
Ni^{2+}	25	32.15	38,886	0.663	0.983	9.95	0.724	0.990
	35	33.48	41,600	0.709	0.981	10.81	0.721	0.990
	45	34.51	45,007	0.767	0.980	11.66	0.715	0.991
Cr(VI)	25	22.56	76,470	1.471	0.967	9.501	0.538	0.994
	35	23.54	77,760	1.496	0.962	9.867	0.542	0.995
	45	24.55	78.948	1.518	0.959	10.24	0.548	0.996
As(V)	25	26.50	93.350	1.246	0.980	10.74	0.612	0.980
	35	28.05	94.136	1.256	0.977	11.35	0.618	0.982
	45	29.61	95.542	1.275	0.973	12.01	0.624	0.983

adsorption process of studied pollutants on AS3-PAN. For the sample AS3-PAN, the values of q_{max} and b are increased with the increase of temperature, which means that the adsorption capacity of Cd^{2+} and Pb^{2+} is higher at higher temperatures, while the standard error for these parameters remained almost identical. Adsorption isotherms of Cd^{2+}, Pb^{2+} and Ni^{2+} ions on AS3-PAN, at 25°C, 35°C and 45°C, are shown in Fig. S4.

The results presented in Table 7 indicate that different factors such: ion size, affinity and hydration shell structure of the cation cause changes in capacity values. On the other hand, binding capabilities of AS3-PAN depend on: (i) the functionalities present on adsorbent surface, (ii) affinity/binding ability of these groups, and (iii) the present adsorbate species (Figs. S2 and S3), first and the last being pH dependent parameters. The speciation diagram showed presence of M^{2+} (Fig. S2), and appropriate equilibria of $HCrO_4^-$/CrO_4^{2-} and $H_2AsO_4^-$/$HAsO_4^{2-}$ ions (Fig. S3) at operative pH. The adsorption of metal ions onto amino modified adsorbents was attributed to the primary and secondary amine groups. Hydrolysis of PAN causes different transformation in surface/interior functionalities, that is, hydrolysis of ester/cyano groups and condensation with formation of imino sequences (Fig. 1.), which also participate in adsorption processes influencing adsorption efficiency [34,35].

The simple indicators which quantitatively describe success of adsorption are coefficient b and separation factor R_L. High value of coefficient b indicates that AS3-PAN can be used for the removal of Cd^{2+} and Pb^{2+} ions from natural water to obtained moderate to high purity water. Also, separation factor R_L, calculated according to Eq. (2), is used for evaluation of the feasibility of adsorption:

$$R_L = \frac{1}{(1 + bC_i)} \quad (2)$$

where C_i (mol dm^{-3}) is initial adsorbate concentration and b (dm^3 mol^{-1}) is Langmuir constant. Value of R_L points out to the isotherm type: irreversible (R_L = 0), favorable (0 < R_L < 1),

Table 8
Thermodynamic parameters for the adsorption of selected ions on AS3-PAN

	$\Delta G°$ (kJ mol^{-1})			$\Delta H°$ (kJ mol^{-1})	$\Delta S°$ (J mol^{-1} K^{-1})	R^2
	298 K	308 K	318 K			
Cd^{2+}	–41.30	–42.79	–44.30	2.66	149.95	0.996
Pb^{2+}	–44.22	–45.85	–47.51	4.09	164.77	0.994
Ni^{2+}	–35.55	–36.93	–38.35	5.57	140.24	0.996
Cr(VI)	–37.19	–38.51	–39.82	1.22	131.03	0.998
As(V)	–38.32	–39.63	–40.96	0.91	131.59	0.968

linear (R_L = 1), unfavorable (R_L > 1). R_L for the adsorption of Cd^{2+}, Pb^{2+}, Ni^{2+}, Cr(VI) and As(V) on AS3-PAN is in range from 0.026 to 0.739, from 0.013 to 0.598, from 0.115 to 0.937, from 0.061 to 0.871, and from 0.071 to 0.887, respectively, indicating that the adsorption of studied pollutants on AS3-PAN are favorable processes. These results are in accordance with the values of Freundlich adsorption intensity parameter 1/*n*. Obtained adsorption results clearly indicate the differences in binding capability of AS3-PAN with respect of ionic species of studied ions.

The adsorption and kinetic results indicate a complex adsorption processes/binding mechanism which relates to the co-existence of mainly physisorption, that is, mainly electrostatic attraction and ion exchange, and chemisorption, that is, chelation/complexation to overall adsorption processes. Schematic presentation of the possible bonding mechanism is given in Fig. 5.

Binding capacity/energy of amino groups was estimated from theoretically calculated potential curves for cyclic Cd-ethylene diamine (Cd/cis-EDA) and non-cyclic (Cd/trans-EDA) complexes. Binding and total energy is larger for cyclic, both the triplet and singlet state over the distances considered. The more stabilized Cd(cis-EDA) exciplex, caused by the coordination of two N atoms to the delocalized *p* electron of Cd atom, was also accompanied by appropriate structural arrangement/adaptation from the non-cyclic to cyclic structure [36].

Cadmium(II) EDA (N-donor ligands) complexes, analyzed using ^{113}Cd NMR spectra showed that, except $[Cd(H_2O)_6]^{2+}$, and hydrated mono, bis and tris Cd/EDA complexes, that is, $[Cd(EDA)]^{2+}$, $[Cd(EDA)_2]^{2+}$ and $[Cd(EDA)_3]^{2+}$, respectively, was beneficially formed at basic pH. Higher coordination ability of EDA appeared due to ionization constants pK_{a1} and pK_{a2} of 7.19 and 9.92, respectively. Higher stability of $[Cd(EDA)]^{2+}$ (log K_1 = 5.47) with respect to 4.55 and 2.07 for bis and tris complexes indicated that analogous complexes of adsorbed ions are present at adsorbent surface [37].

Adsorption mechanism of As(V) on aminated material, prepared by surface-initiated atom transfer radical polymerization, was studied according to the results obtained from X-ray photoelectron spectroscopy (XPS) spectra. As(V) and Cr(VI) removal was achieved through electrostatic interaction between the protonated amine groups and anionic species. Also, it has been presented that the adsorption mechanism of Cu(II) and Pb(II), that is, interaction with the amine groups (–NH– and $–NH_2$), by forming chelate structure was undoubtedly evidenced by XPS results [38]. Presented results suggest that main binding mechanism of the metal cations on AS3-PAN is coordination/complexation (high significance), electrostatic interactions (lower), and specific interactions (minor). Oppositely, the oxyanions create dominantly electrostatic interactions.

Thermodynamic aspect of adsorption process is analyzed from Gibbs free energy ($\Delta G°$), enthalpy ($\Delta H°$) and entropy ($\Delta S°$) calculation using Van't Hoff Eqs. (3) and (4):

$$\Delta G° = -RT\ln(b) \tag{3}$$

$$\ln(b) = \frac{\Delta S°}{R} - \frac{\Delta H°}{(RT)} \tag{4}$$

where T is absolute temperature in K, and R is universal gas constant (8.314 J mol^{-1} K^{-1}). Langmuir adsorption constant b is calculated from isothermal experiments (Table 7). $\Delta H°$ and $\Delta S°$ are calculated from slopes and interceptions in diagram $\ln(b) - T^{-1}$, assuming that the system attained stationary conditions. The quality of data fitting is confirmed with high R values and low values of standard errors (Table 8).

Negative $\Delta G°$ values (Table 8), point out that the adsorption of all ions on AS3-PAN is a spontaneous process, with higher spontaneity obtained at higher temperature. It is known that cation/oxyanion species in water can be present in the forms of multilayered hydrated ions, charged or neutral. Moreover, the change of solution pH is followed by ionic species change affecting structure/extent of interaction in hydration shell. Regardless on coordination properties, solvated cations are more easily desolvated at higher temperatures, the diffusion through boundary layer and inside the pores takes place at higher diffusional rate. Generally, the change of free energy for physisorption lies between –20 and 0 kJ mol^{-1}, both physisorption and chemisorption in the range from –20 to –80 kJ mol^{-1}, while values between –80 and –200 kJ mol^{-1} correspond to chemisorption. Thus, the interaction between selected ions with AS3-PAN could be described by contribution of both physisorption and chemisorption processes.

The $\Delta H°$ does not vary much between analysed ions, with slight tendency to be low for oxyanions. Contribution to possible explanation of a low endothermic nature of the process could be that solvated ion, that is, $[M(H_2O)_6]^{2+}$, and amino groups at AS3-PAN surface need energy to be desolvated in order to readily interact. The formation of an M^{2+}/

EDA complexes takes place by breaking of an M^{2+}--O bond and the formation of an M^{2+}--N bond strikingly influencing overall enthalpy change since the process is exothermic [39]. Oppositely, endothermic nature of desolvation process exceeds this energy, and together with contribution of energetic effect of other elementary processes, either exothermic or endothermic; in summary low positive values of $\Delta H°$ was obtained [9].

Positive values of entropy change ($\Delta S°$) indicate the increase in disorder (randomness) on boundary solid-liquid surface. Water molecules in surrounding solvation shell of metal ion are polarized/oriented to the ion forming mutual hydrogen-bonded water molecules contributing to system orderliness. Amino/hydrophilic groups strongly interact with water molecules by creating hydrogen bonds. The formation of M^{2+}/amino group complexes was followed by liberation of water molecules from adsorbent surface and from cation hydration shell. Both processes contribute to $\Delta S°$ increases. On the other hand, decrease in translational, rotational and vibrational motion due to formation of the chelate ring is reflected in entropy decrease. This process is significant in initial period, and this factor diminishes in the course of progress of adsorption. According to this, higher entropy of complex formation means their higher stability, and this result indicates better interaction/higher stability of M^{2+}/amino group complexes.

3.9. Isosteric heat of adsorption

The design of adsorption processes needs measurable data such as temperature, equilibrium constant, and ones calculated based on experimental data: activation energy and activation parameters (sections 3.3.1 and 3.3.2), and Gibb's free energy change, enthalpy, entropy (section 3.5), and isosteric heat of adsorption is also required. These parameters are input design parameters in evaluating/calculating the performance, analysis of the mechanism of an adsorption/separation processes and optimization of an adsorption process. Isosteric heat of sorption ($\Delta_{iso}H$) is defined as the heat determined at constant amount of adsorbed adsorbate. It represents one of the basic requirements for the characterization and optimization of any sorption process. $\Delta_{iso}H$ was calculated using the Clausius–Clapeyron Eq. (5):

$$\frac{d\left(\ln C_e\right)}{dT} = \frac{\Delta_{iso}H}{RT^2} \tag{5}$$

For this purpose, the equilibrium concentration (C_e) at constant amount of Pb^{2+}, Cd^{2+}, Ni^{2+}, Cr(VI) and As(V) ions sorbed is obtained from the isotherm data at different temperatures (Fig. 6), while $\Delta_{iso}H$ values were obtained from the slope of $\ln C_e$ versus $1/T$ plot for different amounts of sorbate onto the AS3-PAN (Fig. 6).

The plots of ln C_e vs. $1/T$ were found to be linear with high R^2 values of presented isosteres (Fig. 7). The heat of physical adsorption, which involves only relatively weak intermolecular forces such as van der Waals and electrostatic interactions, is low compared with that of chemisorption, which involves essentially the formation of a chemical bond between the adsorbate and active sites at surface of the adsorbent. The upper limit for physical adsorption may be higher than 80 kJ mol^{-1} for adsorption on adsorbents. The heat of chemisorption ranges from over 400 kJ mol^{-1} to less than 80 kJ mol^{-1} [40]. The values of $\Delta_{iso}H$ ranged from 3.91 to 4.62, 4.79 to 6.11, 3.51 to 9.76 and 3.63 kJ mol^{-1} indicate that the adsorption of of Pb^{2+}, Cd^{2+}, Ni^{2+}, Cr(VI) and As(V) ions respectively onto AS3-PAN is a physical process, that is, mostly electrostatic interactions.

3.10. Desorption study

Synthesized adsorbents were subjected to reusability study by variation of process parameters: concentration and regenerator type in order to decrease/minimize effluent polluted water generation. Desorption percentage of Cd^{2+}, Pb^{2+} and Ni^{2+} ions steady increases with the increasing of pH value when sodium hydroxide is used as desorption agent, and reaches maximum >92% at pH > 9. Somewhat lower efficiency is obtained using sodium hydrogen carbonate. Thus, two goals are achieved using the base as desorption agent: regeneration and deprotonation of ammonium group. Results of

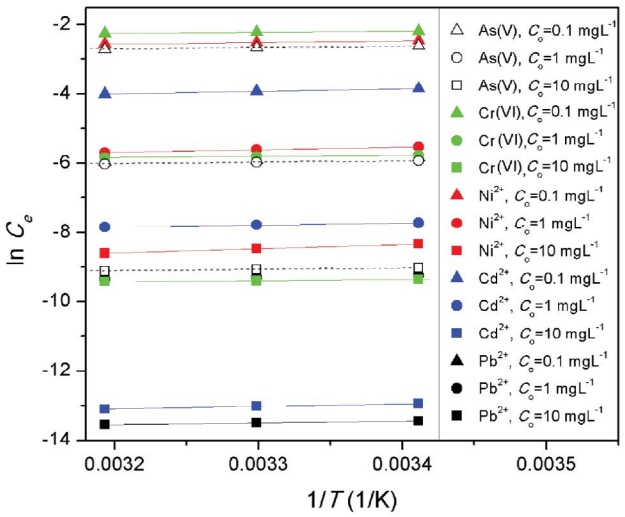

Fig. 6. Linearized plots of ln C_e versus $1/T$ for adsorption of Pb^{2+}, Cd^{2+}, Ni^{2+}, Cr(VI) and As(V) ions onto AS3-PAN.

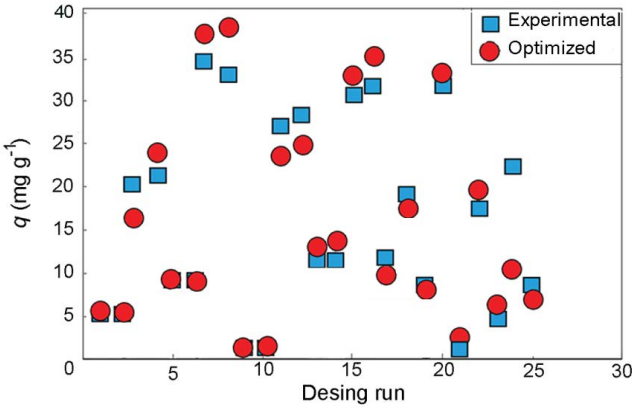

Fig. 7. Experimental and optimized data for the adsorption of Cd^{2+} on AS3-PAN.

Table 9
Results of five adsorption-desorption cycles for the AS3-PAN/pollutant system [$C_i[_{Cd}{}^{2+}] = C_i[_{Pb}{}^{2+}] = 0.963$ mg L^{-1}, $C_i[_{Ni}{}^{2+}] = 1.01$ mg L^{-1}, $C_{i[As(V)]} = C_{i[Cr(VI)]} = 1.05$ mg L^{-1}, $m/V = 200$ mg L^{-1}, $T = 25$°C]

Adsorbent/Recycle step		1	2	3	4	5
Cd^{2+}	Adsorption (%)	91.2	88.1	86.6	82.5	79.2
	Desorption (%)	89.8	89.7	87.9	85.8	82.1
Pb^{2+}	Adsorption (%)	90.5	89.7	86.3	81.7	79.5
	Desorption (%)	89.1	86.4	85.6	82.7	80.4
Ni^{2+}	Adsorption (%)	83.3	79.4	75.5	74.1	70.2
	Desorption (%)	88.5	85.4	82.7	81.4	78.5
As(V)	Adsorption (%)	82.7	80.3	79.1	76.4	71.8
	Desorption (%)	90.1	88.7	86.4	84.3	81.7
Cr(VI)	Adsorption (%)	81.7	79.4	77.8	73.1	69.8
	Desorption (%)	89.9	88.7	85.4	82.4	80.1

Desorption solution: 4% $NaHCO_3$ and 2% NaCl

desorption study, performed in acidic condition at pH < 5, show also high desorption efficiency. As example, AS3-PAN loaded with Cd^{2+} shows 96% leaching capacity with EDTA, 94% with oxalic acid, and 96 % with citric in the first regeneration step. The hexadentate complexing leachates EDTA and citric acid show best chelating capabilities. Significant disadvantage of the desorption based on acidic regenerator arise from necessary deprotonation of ammonium terminal group to restore its adsorption potential. Thus, the results of desorption study, using 4% $NaHCO_3$ and 2% NaCl, is presented in Table 9.

Obtained results indicate that AS3-PAN can be consecutively used in a successive adsorption/desorption processes of the removal of heavy metal ions/oxyanions from water. Adsorption capability of AS3-PAN shows gradual removal efficiency decrease as a consequence of organic structure, that is, amide bond, hydrolysis. These processes bring to decrease of amino value (AN): after fifth cycle 0.96 mmol g^{-1} (Cd^{2+}) and 0.102 mmol g^{-1} (As(V)) were found. After the regeneration processes, regarding As(V) and Cr(VI) ions, the collected spent effluent solution contained relatively low amount of arsenic/chromium indicates necessitate design of appropriate technology for the treatment of collected effluent into a non-hazardous material suitable for landfilling. Pollutant removal could be achieved using (a) affinity adsorption, (b) reaction with iron (precipitation of $Fe(H_2AsO_4)_3$ in pH range 2–7), and (c) reaction with calcium (precipitation of $Ca(H_2AsO_4)_2{\cdot}nH_2O$ in pH range 2–7) [41,42]. The effective technology for safe disposal of desorption solution and washing medium could be treated by iron(III) chloride or calcium(II) chloride solution (5%) with pH adjustment to neutral pH using 5% hydrochloric acid. The addition of iron ion helps precipitation of heavily soluble As(V) and Cr(VI) salts. After 12 h, a heavy dark brown precipitate is formed, which could be easily filtered using a combination of sand filters mixed with filtration aid - diatomaceous earth.

3.11. Effect of interfering ions

Model water, spiked with 100 μg L^{-1} of the selected pollutants and competitive ions at concentration found in natural water (Table S5), is used in competitive study. Obtained results are given in Tables 10 and 11. Tolerable limit was defined as the highest amount of foreign ions that produced an error not exceeding ±5% in the determination of analyte ions.

Interfering ions in different interference-to-analyte ratios were added individually to 50 mL of solutions containing 100 μg L^{-1} of lead and cadmium ions, followed by applying the method discussed above. Significant interference was noticed from the results of competitive study in the system spiked with studied cation or oxyanions. Phosphate showed significant influence as a results of amino/phosphate complexes formation. Silica shows significant detrimental effect to adsorption efficiency, while other cations exhibit moderate to low effect. Competitive study of the anions/cations removal from real water sample showed low selectivity of AS3-PAN with respect to cations. Removal efficiency strongly depends on valence state of cations, as well as actual concentration. Higher affinity of trivalent ions, that si, Al^{3+} and Fe^{3+}, with respect to AS3-PAN is defined in competitive adsorption study at equal concentration of ions: two to three-fold higher cations uptake is found with respect to Ni^{2+} while somewhat lower, up to two times, is found with respect to Pb^{2+}.

The separation factor (sf) was used to quantitatively evaluate the degree of selectivity for ion of interest in presence of coexisting ions [43], according to Eq. (6) exemplified for Cd^{2+}:

$$\mathrm{sf}_i^{\mathrm{Cd}} = \frac{q_{e,\mathrm{Cd}} C_{e,i}}{q_{e,i} C_{e,\mathrm{Cd}}} \tag{6}$$

where $C_{e,\mathrm{Cd}}$ and $C_{e,i}$, as well as $q_{e,\mathrm{Cd}}$ and $q_{e,i}$ are the equilibrium concentration and capacities of Cd^{2+} and coexisting ion i, respectively, (mmol g^{-1}). For sf = 1 selectivity for Cd^{2+} and ion i is equal, while for sf > 1 beneficial Cd^{2+} adsorption in relation to ion i by AS3-PAN could be obtained. Calculated $\mathrm{sf}_{\mathrm{Pb}}^{\mathrm{Cd}}$ and $\mathrm{sf}_{\mathrm{Ni}}^{\mathrm{Cd}}$ values of 0.54 and 2.21 showed somewhat higher affinity of Pb^{2+} and lower of Ni^{2+} in relation to Cd^{2+}, respectively. The $\mathrm{sf}_{\mathrm{Ni}}^{\mathrm{Pb}}$ of 3.4 indicated higher affinity of Pb^{2+} with respect to Ni^{2+}. The low selectivity of AS3-PAN with respect to cations originates form acid/base properties of competitive ions (the hardness and atomic radius) and lone electron pair of hetero atom present in surface functionalities

Table 10
Efficiency of pollutant removal by AS3-PAN in a presence of interfering anion

System	pH_i	Ion[a]/% removal	Content of interfering anions (mg L^{-1})					
			$Cr_2O_7^{2-}$	Cl^-	SO_4^{2-}	F^-	NO_3^-	PO_4^{3-}
Model water[b]	5.6	–	0.4	7.9	18.2	0.10	3.2	16.1
AS3-PAN/model water	8.0	Cd^{2+}/94	0.1	7.7	18.0	0.10	3.0	15.2
	6.1	Pb^{2+}/95	BDL[c]	7.7	18.0	0.10	3.1	15.4
	7.0	Ni^{2+}/91	BDL	7.7	18.1	0.10	3.2	15.1
	6.0	As(V)/90	BDL	7.7	18.1	0.09	3.0	15.5
	6.0	Cr(VI)/92	BDL	7.6	18.2	0.10	3.0	15.5

[a]Percent of pollutant removal (mean value from three determination).
[b]Anion content in water spiked with 100 μg L^{-1} of pollutant without adsorbent.
[c]BDL - below detection limit.

Table 11
Efficiency of pollutant removal by AS3-PAN in a presence of interfering cation

System	pH_i	Ion[a]/% removal	Content of the cations (μg L^{-1})[b]					
			Cu	Ni	Zn	Cd	Pb	Si
Model water[b]	5.5	–	45	20	522	28	55.4	2,089
	8.0	Cd^{2+}/94	37	13	488	7.7[c]	18.9	1,926
	6.1	Pb^{2+}/95	36	12	468	BDL	7.8[c]	1,912
AS3-PAN/modelwater	7.0	Ni^{2+}/91	34	11[c]	492	BDL	15.7	1,889
	6.0	As(V)/90	32	8	444	7	11.7	1,893
	6.0	Cr(VI)/92	31	10	432	8	12.8	1,922

[a]Percent of pollutant removal (mean value from three determination).
[b]Cation content in water spiked with 100 μg L^{-1} of the pollutant of interest.
[c]Spiked with 100 μg L^{-1}.

of AS3-PAN. They contain soft bases, N and O atoms, which are able to create tight interaction with soft heavy metal ions such as Pb^{2+}, Cd^{2+} and Ni^{2+}. Multiple effect of these factors with contribution of both valence state and ion radius dictate complexation ability, and all of these factors influence obtained selectivity. Additionally, effect of interfering ions in real water sample on AS3-PAN adsorption performances is given in Supplementary material. Obtained results indicate possible use of AS3-PAN in an adsorption processes without control of selective pollutant removal.

3.12. Comparison of AS3-PAN adsorbent performance with literature data

Comparison of the literature data of PAN based adsorbents with AS3-PAN give valuable information on the adsorption advantageous/deficiency and their possible application. The q_{max} values of the adsorbents of interest are given in Table 12. Comparison of the adsorption capacities could not be the only mandatory parameters used for evaluation of adsorbent performances. Affinity is, also, an important criterion necessary to be considered in the course of definition of operational conditions. Parameters of economical adsorption technology, with requirements for moderate water purity, should be design to operate to near of the saturation point. It implicates adsorption capacity as major decisive parameter. In the case of requirement for high water purity, the facility should operate "at the left side of the adsorption isotherm", and the adsorption affinity is the most important criterion.

Comparison of q_{max} values shows that thio-functionalized PAN fiber (368.8 mg g^{-1}) [44], hydrolyzed oxidized PAN nanofibers (85.7 mg g^{-1} [45], and PAN/organo bentonite composite (52.6 mg g^{-1}) [46] reach higher q_{max} for Cd^{+2} removal at very high initial Cd^{2+} ions concentration (20.0–500.0 mg L^{-1}) compared with the synthesized amino-terminated waste PAN adsorbent (41.07 mg g^{-1}). The macroporous PAN/hydroxyapatite composite showed low adsorption capacity (6.12 mg g^{-1}) at high initial Cd^{2+} ion concentration (50.0 mg L^{-1}) [47]. Also, hydrolyzed oxidized PAN nanofibers show high adsorption capacity for Pb^{2+} removal (116.2 mg g^{-1}) at high initial Pb^{2+} ion concentration (100.0 mg L^{-1}) [45]. On the other hand, removal of Ni^{2+} on hydrolyzed oxidized PAN nanofibers was lower (21.0 mg g^{-1}) [45] compared with the AS3-PAN fiber. For the As(V) ion removal, the highest q_{max} value is reached for nano-iron oxide nanoparticle loaded PAN nanofibers (851.7 mg g^{-1}) at As(V) ion initial concentration of 5.0 mg L^{-1}

[48]. Molybdenum disulfide modified acid-doped polyaniline/porous PAN nanofibers reach q_{max} of 6.57 mmol g^{-1} for Cr(VI) removal at low initial Cr(VI) ions concentration (2.0 mg L^{-1}) [49]. Comparing maximum adsorption capacities for heavy metal ions/oxyanions removal of similar PAN based adsorbents reported in literature with the heavy metal ions/oxyanions adsorption capacities obtained for AS3-PAN indicate good adsorption performances at applied operational/experimental conditions. Thus, in three-step procedure that was applied on waste PAN, a material of choice for removal of cations in Pb^{2+}, Cd^{+2} and Ni^{2+}, and oxyanions, As(V) and Cr(VI) has been obtained.

3.13. Prediction of the removal of Cd^{2+}, Pb^{2+} and Ni^{2+} ions using AS3-PAN

A four-variable design was used for optimization of adsorption capacity, *q*, using the selected independent parameters. The coded and real values of the independent values are summarized in Table S1. The coefficients of the response function and their statistical significance are evaluated by the least squares method using Design-Expert v.9.0 software, Stat-Ease, Inc. The accurate selection of the equations used for description of the system behavior has a strong influence on the success of the approximation. Obtained functions/equations should provide the whole response surface as accurately as possible, and the most important should be valid in the area of the design space called "region of interest". Thus, among numerous data necessary to be performed to obtain adequate response the experimental design consisted of only 25 runs.

The optimal point for adsorption capacity is predicted using a linear function with the natural logarithm transformation. Used function is fitted to correlate the relationship between the predicted output and the independent variables X_i. Adequacy of the linear regression model is proved by ANOVA test, significance of model coefficients is tested using Student test. The experimental data are analyzed by the response surface regression procedure to fit the following linear model. The full model used in the response (*Y*) is described in the following equation:

$$\ln(Y) = \beta\_0 + \sum\_(i = 1)\text{^}4 \equiv \; [\![\beta\_i \, x\_i \,]\!] \tag{7}$$

where β_0 and β_i are the regression coefficients for intercept and linear terms, respectively; and x_i are the independent variables. ANOVA results indicate that the linear model is significant (*F*-value = 60.01) with standard deviation of 0.45 and with *p*-value < 0.0001. The R^2 value of 0.9231 shows that design data were in good agreement with the experimental data. The predicted R^2 value of 0.8769 is in reasonable agreement with the adjusted R^2 value of 0.9077, with a signal to noise ratio of 25.8. All the variables showed significant effect on the output.

In order to obtain RSM results, polynomial regression modeling is operated between the responses of the corresponding coded values of the four different process variables, and finally, the best model equation for Cd^{2+} and Pb^{2+} ion removal, that is, Eqs. (8) and (S16), respectively, are obtained:

$$\ln(q) = -4.2436 + 0.0068367T + 0.64195\text{pH} + 0.21371C\_i + 0.011432t \tag{8}$$

RSM fitting ANOVA of the adsorption capacity for the adsorption of Cd^{2+} an Pb^{2+} on AS3-PAN are given in Tables 13 and S7, respectively.

The data analysis is realized using hybrid fractional error function (HYBRID); Marquardt's percent standard deviation (MPSD); average relative standard error (ARS); average relative error (ARE); standard error and chemical oxygen demand (COD). The Data Analysis Tools Add-in included in the Microsoft's Excel is used to calculate error functions for available data. The error values for the adsorption of Cd^{2+} and Pb^{2+} on AS3-PAN are given in Tables 14 and S8, respectively.

It was shown that the design of the set of experiments (Table S2) has an important influence on the goodness of the fitting (Tables 12 and S7). The correlation between experimental and designed data adsorption for the Cd^{2+} removal on AS3-PAN is given in Figs. 7 and 8, and also the ones obtained for the adsorption of Pb^{2+} and Ni^{2+} on AS3-PAN given in Figs. S5–S8.

By comparing the figures showing experimental and predicted results, good correlation (Fig. 9) is obtained for the medium values of adsorption variables. The larger

Table 12
RSM fitting ANOVA test for the adsorption of Pb^{2+} on AS3-PAN

q	Sum of squares	Degree of freedom	Mean square	Mean	C.V.[a],%
Model	32.30	4	8.08	1.77	44.90
Residual	12.66	20	0.63	–	–
Total	44.96	24	–	–	–

[a]C.V. – coefficient of variation.

Table 13
RSM fitting ANOVA of the adsorption capacity for the adsorption of Cd^{2+} on AS3-PAN

q	Sum of squares	Degree of freedom	Mean square	Mean	C.V.[a]%
Model	47.71	4	11.93	1.43	31.10
Residual	3.97	20	0.20	–	–
Total	51.68	24	–	–	–

[a]C.V. – coefficient of variation.

Table 14
Values from the error data analysis for the adsorption of Cd^{2+} on AS3-PAN

Errors	Cd^{2+}
HYBRID	68.88
MPSD	50.24
ARS	0.470
ARE	28.27
Standard Error	2.647
COD	0.9311

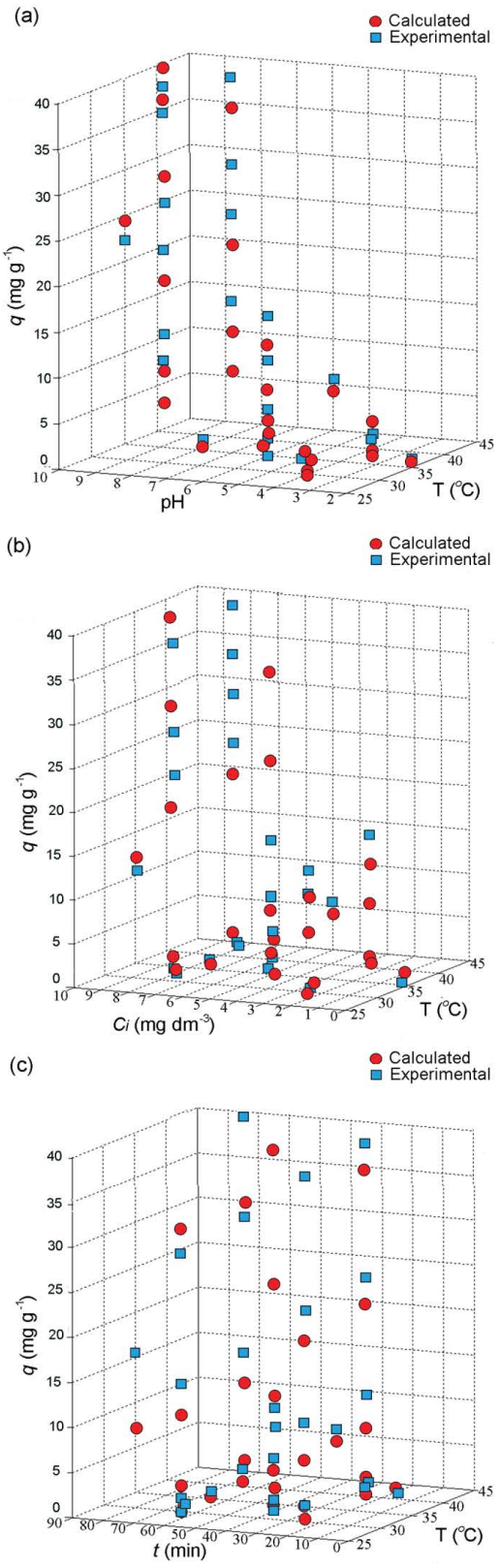

Fig. 8. Correlation between experimental data and design depending on the variable factors, pH value (a), the initial concentration of (b) and the time (c) vs. temperature for Cd^{2+}adsorption.

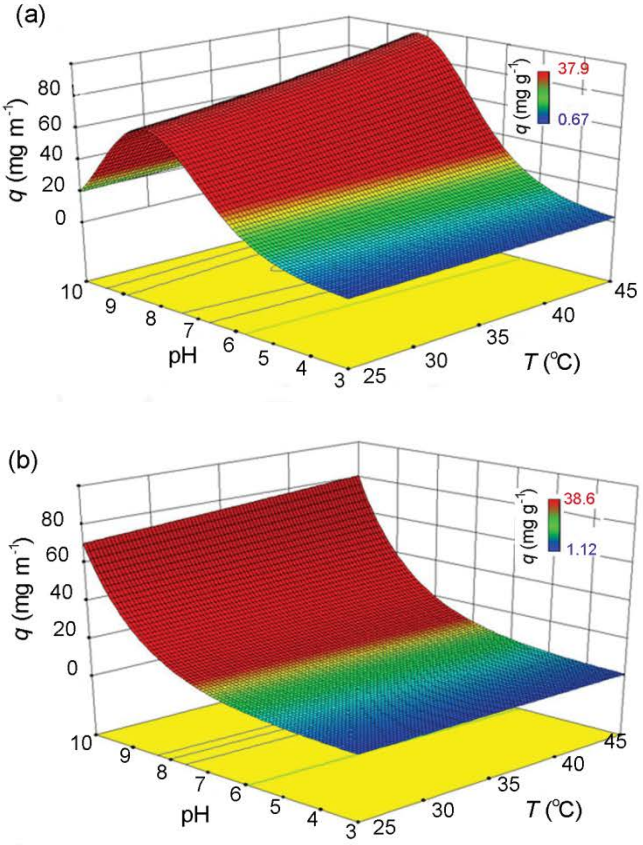

Fig. 9. Comparative view of adsorption capacity versus pH values and temperature for: surface model of experimental data (a) and surface model of predicted data (b) for Cd^{2+} adsorption.

deviation of predicted adsorption capacities values can be noticed at the end of selected range of independent variables (coded values) due to their small participation in the design plan.

The presented results and related discussion indicate that the prediction of adsorption results can be applied in medium range of variable values, whereas at end points larger errors are generated. Hence, one alternative is related to solving this inconsistency by desirable use of reduced variable value ranges for the multi-criterial analysis of adsorption process. On the other hand, good certainty of predicted results could be obtained by including more data in experimental plan in the region of interest. Moreover, obtained results (Fig. 9) provide good prediction in the region of the variable change of highest interest which matches the condition usually/generally found for natural water, that is, pH, and operational temperature. Therefore, first benefit is related to reduction of the large number of necessary experiments, as usual approach in design of adsorption experiments, and on the other side, such methodology provides reliable adsorption data in that way contributing to the environmental protection. This method is reliable in scenarios where fast screening of new adsorbent is required to obtain adsorption results.

4. Conclusion

Modification of waste PAN led to the production of new applicable material in the environmental science for the adsorption of heavy metals from water. In this study, aminated polyacrylonitrile fibers (AS3-PAN) were successfully prepared in three addition/amidation successive steps of PAN waste fibers. Results from adsorption and kinetic study prove high applicability of synthesized adsorbent. Adsorption of cations on AS3-PAN is an intricate process and consists of mainly physisorption with contribution of chemisorption mechanisms. Adsorption capacity of metal ions/oxyanions and the affinity of AS3-PAN are more dependent on surface groups, pH values and temperature than from specific surface, volume and pore diameter. Endothermic nature of adsorption processes indicates that the adsorption capacity concomitantly increase with the temperature raise.

Application of software Design expert 9, with proper design of experimental plan showed that the RSM can be successfully used to predict the adsorption results. This method allows obtaining satisfactory results with a minimization of the number of experiments, that is, 25 instead of 210 experiments, which leads to financial benefit, considering the economic aspect, and minimizing the residuals/waste materials, as the important fact related to the environmental protection. The large overlap of the experimental data and calculated results prove that this method can be successfully used to predict the adsorption results. Certainty of predicted results could be improved by including more data in experimental plan in the region of interest, as it is the condition usually found in natural water, that is, pH, and operational temperature. Thus, main results of this study relates to the use of waste PAN for production of high performance adsorbent used in a limited number of statistically valid experiments providing comprehensive approach in an area of environmental protection. Transformation of waste, using it as raw material for high performance adsorbent synthesis with special care on minimization of additional waste generation, satisfies needs to preserve and improve environmental quality.

Acknowledgment

The authors would like to acknowledge the financial support from the Ministry of Education, Science and Technological Developments of the Republic of Serbia, Project Nos. III45019 and OI172057.

References

[1] A. Ghaffari, S.W. Husain, M.S. Tehrani, M. Anbia, P.A. Azar, Highly efficient adsorption of hexavalent chromium from the aqueous system using nanoporous carbon modified with tetraethylenepentamine, Int. J. Environ. Sci. Technol. 12 (2015) 1835–1844.

[2] N. Obradović, S. Filipović, S. Marković, M. Mitrić, J. Rusmirović, A. Marinković, V. Antić, V. Pavlović, Influence of different pore-forming agents on wollastonite microstructures and adsorption capacities, Ceram. Int., 43 (2017) 7461–7468.

[3] Z.J. Bajić, V.R. Djokić, Z.S. Veličković, M.M. Vuruna, M.Đ. Ristić, N.B. Issa, A.D. Marinković, Equilibrium, kinetic and thermodynamic studies on removal of Cd(II), Pb(II) and As(V) from wastewater using carp (cyprinus carpio) scales, Dig. J. Nanomater. Biostructures, 8 (2013) 1581–1590.

[4] Q.Q. Han, L. Chen, W.X. Li, Z.Y. Zhou, Z. Fang, Z.W. Xu, X.M. Qian, Self-assembled three-dimensional double network graphene oxide/polyacrylic acid hybrid aerogel for removal of Cu^{2+} from aqueous solution, Environ. Sci. Pollut. Res., 25 (2018) 34438–34447.

[5] D. Iannazzo, A. Pistone, I. Ziccarelli, C. Espro, S. Galvagno, S.V. Giofré, R. Romeo, N. Cicero, G.D. Bua, G. Lanza, L. Legnani, M.A. Chiacchio, Removal of heavy metal ions from wastewaters using dendrimer-functionalized multi-walled carbon nanotubes, Environ. Sci. Pollut. Res., 24 (2017) 14735–14747.

[6] J.D. Rusmirović, N. Obradović, J. Perendija, A. Umićević, A. Kapidžić, B. Vlahović, V. Pavlović, A.D. Marinković, V.B. Pavlović, Controllable synthesis of Fe_3O_4-wollastonite adsorbents for efficient heavy metal ions/oxyanions removal, Environ. Sci. Pollut. Res., 26 (2019) 12379–12398.

[7] J.G. Shang, X.R. Kong, L.L. He, W.H. Li, Q.J.H. Liao, Low-cost biochar derived from herbal residue: characterization and application for ciprofloxacin adsorption, Int. J. Environ. Sci. Technol., 13 (2016) 2449–2458.

[8] K. Taleb, J. Markovski, Z. Veličković, J. Rusmirović, M. Rančić, V. Pavlović, A. Marinković, Arsenic removal by magnetite-loaded amino modified nano/microcellulose adsorbents: effect of functionalization and media size, Arabian J. Chem., (2016) (In press), http://dx.doi.org/10.1016/j.arabjc.2016.08.006.

[9] G.D. Vuković, A.D. Marinković, M. Čolić, M.Đ. Ristić, R. Aleksić, A.A. Perić-Grujić, P.S. Uskoković, Removal of cadmium from aqueous solutions by oxidized and ethylenediamine-functionalized multi-walled carbon nanotubes, Chem. Eng. J., 157 (2010) 238–248.

[10] S.B. Deng, R.B. Bai, J.P. Chen, Behaviors and mechanisms of copper adsorption on hydrolyzed polyacrylonitrile fibers, J. Colloid Interface Sci., 260 (2003) 265–272.

[11] G.Q. Huang, W.T. Li, Q. Liu, J.Y. Liu, H.S. Zhang, R.M. Li, Z.S. Li, X.Y. Jing, J. Wang, Efficient removal of uranium(VI) from simulated seawater with hyperbranched polyethylenimine (HPEI)-functionalized polyacrylonitrile fibers, New J. Chem., 42 (2018) 168–176.

[12] S. Deng, P. Wang, G.S. Zhang, Y. Dou, Polyacrylonitrile-based fiber modified with thiosemicarbazide by microwave irradiation and its adsorption behavior for Cd(II) and Pb(II), J. Hazard. Mater., 307 (2016) 64–72.

[13] G. Xu, Y. Zhao, L.P. Hou, J. Cao, M.L. Tao, W.Q. Zhang, A recyclable phosphinic acid functionalized polyacrylonitrile fiber for selective and efficient removal of Hg^{2+}, Chem. Eng. J., 325 (2017) 533–543.

[14] J.S. Markovski, D.D. Marković, V.R. Djokić, M. Mitrić, M.D. Ristić, A.E. Onjia, A.D. Marinković, Arsenate adsorption on waste eggshell modified by goethite, α-MnO_2 and goethite/α-MnO_2, Chem. Eng. J., 237 (2014) 430–442.

[15] X.-L. Shi, Q.Q. Hu, F. Wang, W. Zhang, P. Duan, Application of the polyacrylonitrile fiber as a novel support for polymer-supported copper catalysts in terminal alkyne homocoupling reactions, J. Catal., 337 (2016) 233–239.

[16] J.P.S. Aniceto, S.P. Cardoso, C.M. Silva, General optimization strategy of simulated moving bed units through design of experiments and response surface methodologies, Comput. Chem. Eng., 90 (2016) 161–170.

[17] Z.J. Bajić, Z.S. Veličković, V.R. Djokić, A.A. Perić-Grujić, O. Ersen, P.S. Uskoković, A.D. Marinković, Adsorption study of arsenic removal by novel hybrid copper impregnated tufa adsorbents in a batch system, CLEAN - Soil Air Water, 44 (2016) 1477–1488.

[18] W.J. Chung, S.Y. Chun, S.S. Kim, S.W. Chang, Photocatalytic removal of tetracycline using TiO_2/Ge composite optimized by response surface methodology (RSM), J. Ind. Eng. Chem., 36 (2016) 320–325.

[19] M. Iqbal, N. Iqbal, I.A. Bhatti, N. Ahmad, M. Zahid, Response surface methodology application in optimization of cadmium adsorption by shoe waste: a good option of waste mitigation by waste, Ecol. Eng., 88 (2016) 265–275.

[20] D.A. Jaeger, R. Jose, A. Mendoza, R.P. Apkarian, Surfactant transition metal chelates, Colloids Surf., A, 302 (2007) 186–196.

[21] Z. Veličković, G.D. Vuković, A.D. Marinković, M.S. Moldovan, A.A. Perić-Grujić, P.S. Uskoković, M.D. Ristić, Adsorption of arsenate on iron(III) oxide coated ethylenediamine functionalized multiwall carbon nanotubes, Chem. Eng. J., 181–182 (2012) 174–181.
[22] American Society for Testing and Materials, ASTM D1617-07, Standard Test Method for Ester Value of Solvents and Thinners, 2007.
[23] American Society for Testing and Materials, ASTM D3644, Standard Test Method for Acid Number of Styrene-Maleic Anhydride Resins, 2015.
[24] S. Deng, R.B. Bai, Aminated polyacrylonitrile fibers for humic acid adsorption: behaviors and mechanisms, Environ. Sci. Technol., 37 (2003) 5799–5805.
[25] P. Kampalanonwat, P. Supaphol, Preparation and adsorption behavior of aminated electrospun polyacrylonitrile nanofiber mats for heavy metal ion removal, ACS Appl. Mater. Interfaces, 2 (2010) 3619–3627.
[26] P.K. Neghlani, M. Rafizadeh, F.A. Taromi, Preparation of aminated-polyacrylonitrile nanofiber membranes for the adsorption of metal ions: comparison with microfibers, J. Hazard. Mater., 186 (2011) 182–189.
[27] J. Wang, X.-H. Lv, L. Zhao, J.-P. Li, Removal of chromium from electroplating wastewater by aminated polyacrylonitrile fibers, Environ. Eng. Sci., 28 (2011) 585–589.
[28] S. Mandal, M.K. Sahu, R.K. Patel, Adsorption studies of arsenic(III) removal from water by zirconium polyacrylamide hybrid material (ZrPACM-43), Water Resour. Ind., 4 (2013) 51–67.
[29] M. Abdouss, M. Shoushtari, A. Haji, B. Moshref, Fabrication of chelating diethylenetriaminated pan micro and nano fibers for heavy metal removal, Chem. Ind. Chem. Eng. Q., 18 (2012) 27–34.
[30] Y. Cantu, A. Remes, A. Reyna, D. Martinez, J. Villarreal, H. Ramos, S. Trevino, C. Tamez, A. Martinez, T. Eubanks, J.G. Parsons, Thermodynamics, kinetics, and activation energy studies of the sorption of chromium(III) and chromium(VI) to a Mn_3O_4 nanomaterial, Chem. Eng. J., 254 (2014) 374–383.
[31] Y.S. Ho, G. McKay, Sorption of dye from aqueous solution by peat, Chem. Eng. J., 70 (1998) 115–124.
[32] S. Glasstone, K.J. Laidler, H. Eyring, The Theory of Rate Processes, McGRAW-HILL Book Company, New York, 1941.
[33] K.Y. Foo, B.H. Hameed, Insights into the modeling of adsorption isotherm systems, Chem. Eng. J., 156 (2010) 2–10.
[34] I.V. Ermakov, A.I. Rebrov, A.D. Litmanovich, N.A. Platé, Alkaline hydrolysis of polyacrylonitrile, 1. Structure of the reaction products, Macromol. Chem. Phys., 201 (2000) 1415–1418.
[35] A.D. Litmanovich, N.A. Platé, Alkaline hydrolysis of polyacrylonitrile. On the reaction mechanism, Macromol. Chem. Phys., 201 (2000) 2176–2180.
[36] O. Takahashi, K. Saito, S. Yamamoto, N. Nishimura, A theoretical study of cadmium-ethylenediamine and -ammonia exciplexes comparison with experiments, Chem. Phys. Lett., 207 (1993) 379–383.
[37] G. Ma, A. Fischer, R. Nieuwendaal, K. Ramaswamy, S.E. Hayes, Cd(II)–ethylenediamine mono- and bimetallic complexes – synthesis and characterization by ^{113}Cd NMR spectroscopy and single crystal X-ray diffraction, Inorg. Chim. Acta, 358 (2005) 3165–3173.
[38] L. Niu, S. Deng, G. Yu, J. Huang, Efficient removal of Cu(II), Pb(II), Cr(VI) and As(V) from aqueous solution using an aminated resin prepared by surface-initiated atom transfer radical polymerization, Chem. Eng. J., 165 (2010) 751–757.
[39] P. Paoletti, Formation of metal complexes with ethylenediamine: a critical survey of equilibrium constants, enthalpy and entropy values, Pure Appl. Chem., 56 (1984) 491–522.
[40] M. Doğan, M. Alkan, Adsorption kinetics of methyl violet onto perlite, Chemosphere, 50 (2003) 517–528.
[41] D. Mohan, C. Pittman, Activated carbons and low cost adsorbents for remediation of tri- and hexavalent chromium from water, J. Hazard. Mater., 137 (2006) 762–811.
[42] D. Mohan, C.U. Pittman, Arsenic removal from water/wastewater using adsorbents-a critical review, J. Hazard. Mater., 142 (2007) 1–53.
[43] D.J. Malik, V. Strelko, M. Streat, A.M. Puziy, Characterisation of novel modified active carbons and marine algal biomass for the selective adsorption of lead, Water Res., 36 (2002) 1527–1538.
[44] S. Deng, G. Zhang, S. Liang, P. Wang, Microwave assisted preparation of thio-functionalized polyacrylonitrile fiber for the selective and enhanced adsorption of mercury and cadmium from water, ACS Sustainable Chem. Eng., 5 (2017) 6054–6063.
[45] S.H. Lee, Y.G. Jeong, Y.I. Yoon, W.H. Park, Hydrolysis of oxidized polyacrylonitrile nanofibrous webs and selective adsorption of harmful heavy metal ions, Polym. Degrad. Stab., 143 (2017) 207–213.
[46] T.S. Anirudhan, M. Ramachandran, Synthesis and characterization of amidoximated polyacrylonitrile/organobentonite composite for Cu(II), Zn(II), and Cd(II) adsorption from aqueous solutions and industry wastewaters, Ind. Eng. Chem. Res., 47 (2008) 6175–6184.
[47] X. Wang, B.G. Miin, W.-S. Lyo, V. Chihaia, M. Gartner, T. Stoica, J.Y. Bae, S.-H. Suh, Column study of cadmium adsorption onto polyacrylonitrile/hydroxyapatite, Rev. Roum. Chim., 55 (2010) 443–447.
[48] D. Morillo, M. Faccini, D. Amantia, G. Pérez, M.A. García, M. Valiente, L. Aubouy, Superparamagnetic iron oxide nanoparticle-loaded polyacrylonitrile nanofibers with enhanced arsenate removal performance, Environ. Sci. Nano, 3 (2016) 1165–1173.
[49] J. Qiu, F. Liu, S. Cheng, L. Zong, C. Zhu, C. Ling, A. Li, Recyclable nanocomposite of flowerlike MoS_2@hybrid acid-doped PANI immobilized on porous PAN nanofibers for the efficient removal of Cr(VI), ACS Sustainable Chem. Eng., 6 (2018) 447–456.

Supporting information

S1. Experimental part

S1.1. Methods used for material characterization

$$\Delta w(\%) = \left(\frac{w_g - w_0}{w_0} \right) \quad \text{(S1)}$$

The conversion degree of amino groups on PAN fibres is calculated according to Eq. (S2):

$$\text{Conversion}(\%) = \left(\frac{w_g - w_0}{w_0} \right) \times \frac{M_0}{M_1} \times 100 \quad \text{(S2)}$$

where: w_0 and w_g weights of raw and modified PAN fibres; M_0 – molecule mass of acrylonitrile monomer; and M_1 – DETA molecule mass.

S1.2. Batch adsorption experiment

$$\Delta q(\%) = \sqrt{\sum \frac{\left[\frac{\left(q_{\text{exp}} - q_{\text{cal}} \right)}{q_{\text{exp}}} \right]^2}{N-1}} \times 100 \quad \text{(S3)}$$

where q_{exp} and q_{cal} are experimental and calculated amounts of Cd^{2+}, Pb^{2+}, Ni^{2+}, Cr(VI) and As(V) ions adsorbed on AS3-PAN, and N is the number of data used in the analysis.

S1.3. Design of adsorption experiments using response surface methodology

Table S1
Coded and real values of independent variables for the optimization design of Cd^{2+} adsorption on AS3-PAN

Independent variable	Coded and real values				
	–2	–1	0	1	2
Temperature, X_1 (°C)	25	30	35	40	45
pH value, X_2	2	4	6	8	10
Initial concentration, X_3 (mg L^{-1})[a]	0.1	2.5	5	7.5	10
Time, X_4 (min)	5	25	45	65	90

[a]Constant ratio of adsorbent dosage vs. adsorbate solution was used.

Table S2
Experimental plan for Cd^{2+} adsorption on AS3-PAN adsorbent

No.	X_1, T (°C)	X_2, pH	X_3, C_i (mg L^{-1})	X_4, t (min)
1	30	4	2.5	25
2	40	4	2.5	25
3	30	8	2.5	25
4	40	8	2.5	25
5	30	4	7.5	25
6	40	4	7.5	25
7	30	8	7.5	25
8	40	8	7.5	25
9	30	4	2.5	65
10	40	4	2.5	65
11	30	8	2.5	65
12	40	8	2.5	65
13	30	4	7.5	65
14	40	4	7.5	65
15	30	8	7.5	65
16	40	8	7.5	65
17	25	6	5	45
18	45	6	5	45
19	35	2	5	45
20	35	10	5	45
21	35	6	0.1	45
22	35	6	10	45
23	35	6	5	5
24	35	6	5	90
25	35	6	5	45

S1.3.1. FTIR analysis

S1.4. Influence of solution pH on adsorption efficiency

Speciation diagram of Ni^{2+}, Cd^{2+} and Pb^{2+} are given on Fig. S2, while speciation diagrams of oxyanions, that is, As(V) and Cr(VI), are given on Fig. S3.

As example lead species in water solution could be present in the forms of Pb^{2+}, $Pb(OH)^+$, $Pb(OH)_2$ and $Pb(OH)_3^-$ at different pH values. Equilibrium concentrations of Pb^{2+} ionic species, at different pH, could be calculated from appropriate constants (log K) for hydrolysis reactions [S6] at 25°C and the precipitation constant of $Pb(OH)_2(s)$ (1.2×10^{-15}) (given on Fig. S2). Precipitated $Pb(OH)_2$ at pH higher than 8 was determined theoretically and experimentally and subtracted from the overall available amount of Pb^{2+} ions, and thus reliable values of adsorbed Pb^{2+} were obtained (Fig. S2). Similar methodology was applied for Cd^{2+} and Ni^{2+} ion.

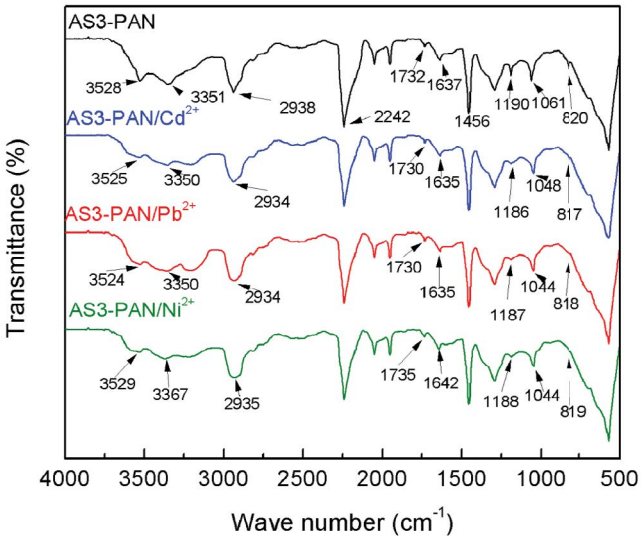

Fig. S1. FTIR spectra of AS3-PAN before and after the adsorption of Cd^{2+} (a), Pb^{2+} (b) and Ni^{2+} (c) [$C_i[_{Cd}{}^{2+}]$ = 5.12 mg L^{-1}, $C_i[_{Pb}{}^{2+}]$ = 4.82 mg L^{-1}, $C_i[_{Ni}{}^{2+}]$ = 5.00 mg L^{-1}, m/V = 100 mg L^{-1}, pH = 6 ± 0.2 and T = 25°C].

S1.5. Time-dependent adsorption study

S1.5.1. Adsorption kinetic

Complex adsorption process, due to contribution of mass transfer and chemical reaction to overall mechanism, was usually described by using different kinetic models or adsorption diffusion models:

The pseudo-first-order, that is, Lagergren rate equation, is based on solid capacity. Its linear form is given by the following Eq. (S4) [S7]:

$$\ln\left(q_e - q_t\right) = \ln q_e - k_1 t \tag{S4}$$

where k_1 (min^{-1}) is the pseudo-first rate constant, q_t (mg g^{-1}) is the adsorption capacity at time t (min), and q_e (mg g^{-1}) is the value of adsorption capacity at equilibrium.

The linear form of pseudo-second-order equation [S8] is expressed by Eq. (S5):

$$\frac{t}{q_t} = \frac{1}{k_2 q_e^2} + \frac{1}{q_e} t \tag{S5}$$

where k_2 (g mg^{-1} min^{-1}) is the second-order rate constant, q_t (mg g^{-1}) and q_e (mg g^{-1}) are the adsorption capacities at any time t and at equilibrium, respectively.

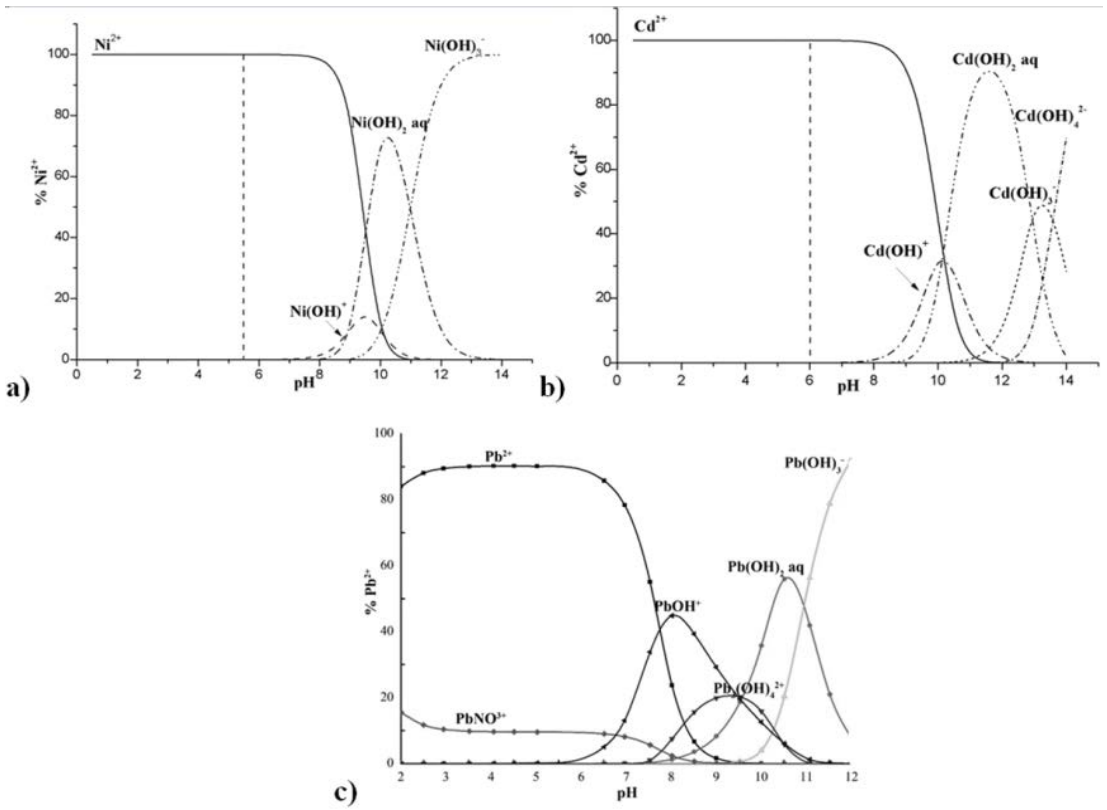

Fig. S2. pH dependent speciation of (a) Ni^{2+}, (b) $Cd^{2+}$and (c) Pb^{2+} ions.

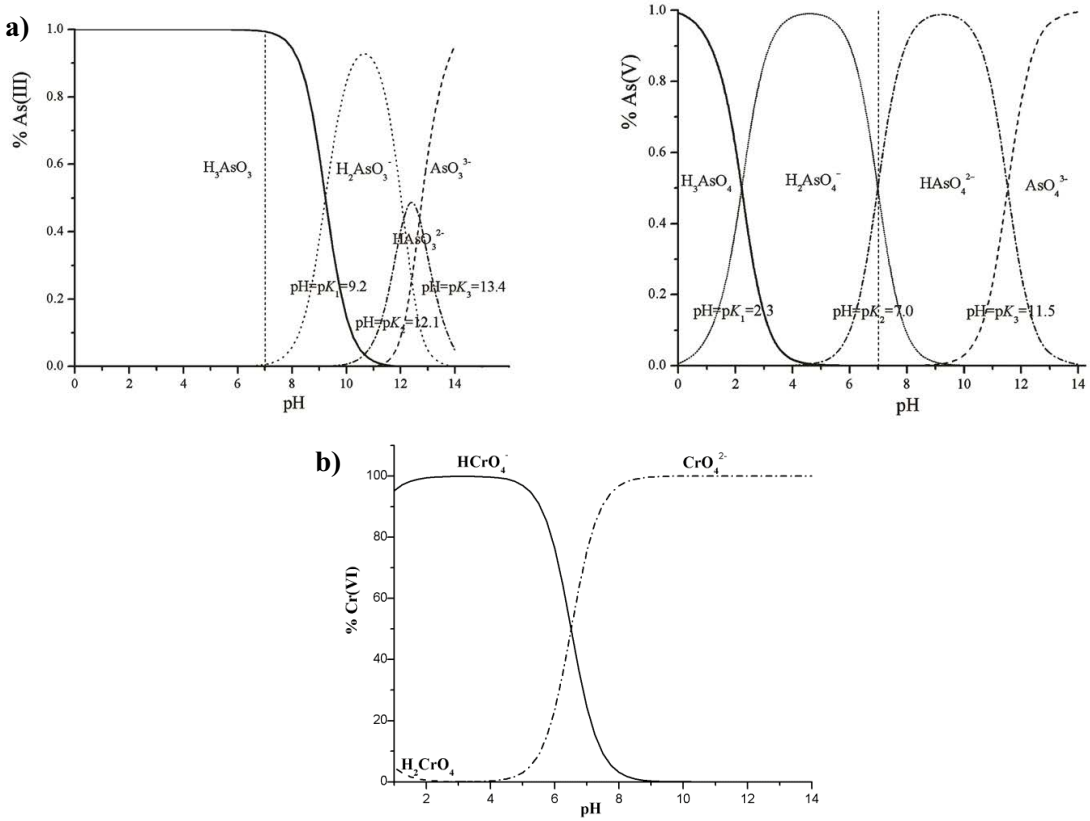

Fig. S3. pH dependent speciation of (a) arsenate and (b) chromate.

The initial sorption rate h_2 (mg g^{-1} min^{-1}) at $t \to 0$ is calculated as:

$$h_2 = k_2 q_e^2 \tag{S6}$$

In order to elucidate the possible chemisorption process for systems with heterogeneous adsorbing surface, the following simplified form of Elovich equation [S9] was used:

$$q_t = \frac{1}{b}\ln(ab) + \frac{1}{b}\ln t \tag{S7}$$

where q_t (mg g^{-1}) represents the adsorption capacity at any time t, a is initial copper adsorption rate (mg g^{-1} min^{-1}), while b is related to the extent of surface coverage and activation energy for chemisorption (g mg^{-1}). An approaching equilibrium factor R_E obtained from dimensionless Elovich equation [S10] is defined as:

$$R_E = \frac{1}{q_{\text{ref}} b} \tag{S8}$$

where q_{ref} is the solid phase concentration at time t_{ref} which is the longest time in adsorption process. According to classification of characteristic curves based on R_E derived from the Elovich equation [S10], there are four type of characteristic curves, depending on R_E value: if $R_E > 0.3$, then the curve rises slowly; if R_E is between 0.1 and 0.3, the curve rises mildly (mild adsorption); the value of R_E between 0.02 and 0.1 indicate rapid adsorption and when $R_E < 0.02$, the curve instantly approaches equilibrium.

Multi step nature of adsorption processes could be controlled by bulk diffusion, boundary layer diffusion, intra-particle diffusion and surface adsorption. The first steep linear part demonstrates external mass transfer from bulk solution to the most available adsorptive sites at outer adsorbent surface. The second and the third parts of the adsorption process significantly depend on adsorbent porosity, that is, pore structure and geometry and network density. Due to the concentration gradient, the ions diffuse through bulk solution and treelike system of macro-, meso- and micropores, extending into adsorbent interior to reach all available surface active sites. The intra-particle resistance slows down adsorbate transport, that is, net transport in a direction of variable time-dependent concentration gradient. At the final stage of process, the adsorption takes place at low rate until the saturation of all available surface sites is achieved.

In the case where internal diffusion is the rate-limiting step, then the kinetic data can be well correlated using following Weber and Morris equation [S11]:

$$q_t = k_i t^{1/2} + C \tag{S9}$$

where k_i (mg g^{-1} min$^{-1/2}$) is intraparticle diffusion rate constant and C is constant related to the thickness or boundary layer. If the intraparticle diffusion is the sole rate-limiting step, then the plot of q_t vs. $t^{1/2}$ would result in a linear relationship and would pass through the origin. The values of intraparticle diffusion rate k_i, and C can be obtained from the slope of q_t versus $t^{1/2}$ plot. Other kind of kinetic models was proposed by Dunwald-Wagner (DW) model given by Eqs. (S10) and (S11):

$$\frac{q}{q_e} = 1 - \frac{6}{\pi^2}\sum_{n=1}^{\infty}\frac{1}{n^2}\exp\left[-n^2 K t\right] \tag{S10}$$

where K (min^{-1}) is the rate constant of adsorption. Simplification of the Eq. (S10) gave:

$$\log\left(1 - \left(\frac{q}{q_e}\right)^2\right) = -\frac{K}{2.303}t \tag{S11}$$

A plot of $\log(1-(q/q_1)^2) \sim t$ should give linear plot and the rate constant can be calculated from the slope of correlation line. DW was reasonably used to describe different kinds of adsorption systems and estimation of adsorption kinetics.

A typical intra-particle diffusion model is the homogeneous solid diffusion model (HSDM), which can describe mass transfer in an amorphous and homogeneous sphere [S12], and can be presented by following differential equation:

$$\frac{\partial q}{\partial t} = \frac{D_s}{r^2}\frac{\partial}{\partial r}\left(r^2\frac{\partial q}{\partial r}\right) \tag{S12}$$

where D_s is intraparticle diffusion coefficient, r radial position, and q the time-dependent adsorption capacity. Exact solution to Eq. (S12) for the defined adsorption condition (neglected external film resistance) was given by Crank [S13] as follows:

$$\frac{q}{q_s} = 1 + \frac{2R}{\pi r}\sum_{n=1}^{\infty}\frac{(-1)^n}{n}\sin\frac{n\pi r}{R}\exp\left[\frac{-D_s t\pi^2 n^2}{R^2}\right] \tag{S13}$$

S1.6. Adsorption study

Langmuir and Freundlich isotherms are the most commonly used model for fitting of adsorption data. Langmuir isotherm means the formation of monolayer on the homogeneous adsorption surface and the adsorption of each molecule have equal adsorption activation energy. Freundlich isotherm signifies heterogeneous surface with uneven adsorption heat distribution with the possibility of the existence of multi-layered adsorption [S1].

$$q = \frac{bq_{\max}C}{1+bC}\text{, or linear form } \frac{C}{q} = \frac{1}{bq_{\max}} + \frac{C}{q_{\max}} \tag{S14}$$

$$q = k_f C^n\text{, or linear form } \log q = \log k_f + n\log C \tag{S15}$$

where C is equilibrium metal ion concentration left in the solution (mol L^{-1}); q is adsorbed amount of metal ions (mol g^{-1}); $q_{\max}$ and b are Langmuir constants related on the adsorption capacity and adsorption energy. Maximum adsorption capacity, $q_{\max}$, denotes the amount of adsorbate, so the complete adsorption surface is covered with adsorbate

monolayer (mol g^{-1}), and b (L mol^{-1}) is the constant related with the adsorption heat.

In Freundlich model (Eq. (S15)) k_f (mol^{1-n} L^n g^{-1}) is an approximate indicator of the adsorption capacity for the equilibrium concentration, and $1/n$ is the Freundlich adsorption intensity parameter, that is, it defines strength of adsorption. For $n = 1$ the partition between the two phases are independent of the concentration, $1/n < 1$ indicates a normal adsorption, while for $1/n > 1$ indicates cooperative adsorption.

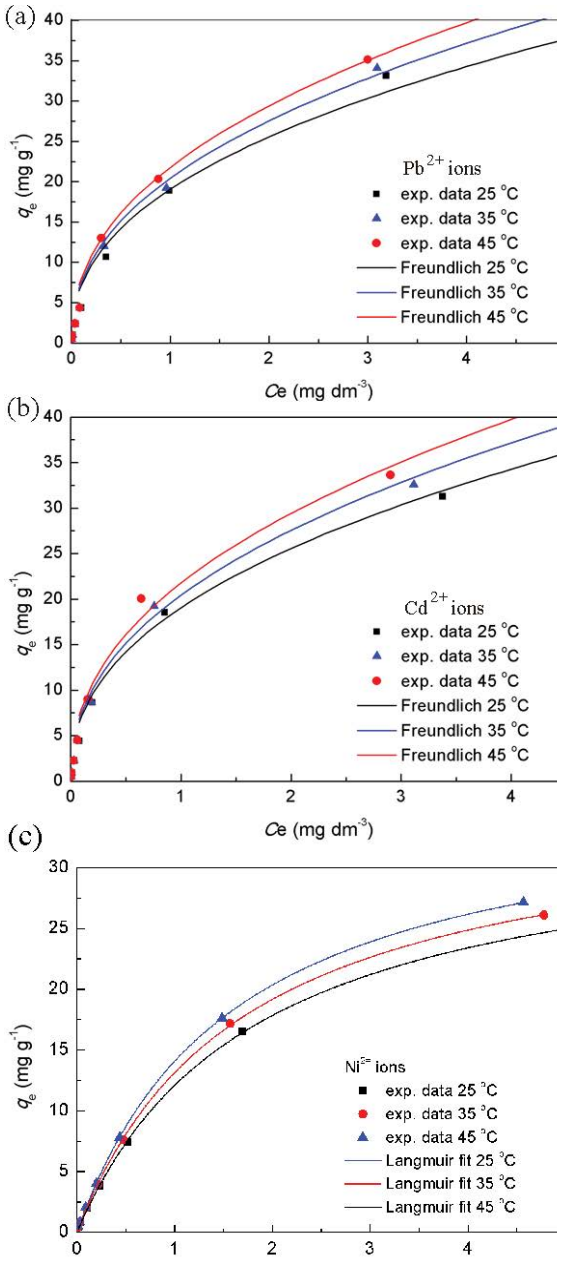

Fig. S4. Isotherms model fitting of the adsorption data of pollutants/AS3-PAN system at 25°C, 35°C and 45°C, m/V = 200 mg L^{-1}, [$C_i[_{Pb}{}^{2+}]$: 0.102; 0.205; 0.512; 0.963; 2.56; 5.12 and 10.24 mg L^{-1}, pH = 6 ± 0.2] (a) $C_i[_{Cd}{}^{2+}]$: 0.096; 0.192; 0.481; 0.963; 1.923; 4.82 and 9.63 mg L^{-1}, pH = 8 ± 0.2 and (b) $C_i[_{Ni}{}^{2+}]$: 0.101; 0.201; 0.505; 1.01; 2.52; 5.04 and 10.08 mg L^{-1}, pH = 7 ± 0.2.

The adsorption parameters calculated using Eq. (S14), the adsorption capacity, q_{max}, and affinity, b, are the most important ones used for analysis of adsorption process and selection of operational conditions. Design of efficient adsorption technology to achieve moderate water purity, will be design to operate to near of the saturation point. It implicates adsorption capacity as major decisive parameter. In the other case, if the requirement is aimed at obtaining of high water purity, the adsorption technology should be design to operate "at the left side of the adsorption isotherm", and the adsorption affinity is decisive factor for technology definition.

Table S3
Dubinin-Radushkevich isotherm parameters for pollutants removal using AS3-PAN

		Dubinin-Radushkevich isotherm			
	T (°C)	q_m (mg g^{-1})	K_{ad} (mol^2 KJ^{-2})	E_a (KJ mol^{-1})	R^2
Cd^{2+}	25	14.14	8.98	7.462	0.838
	35	14.40	8.96	7.469	0.839
	45	14.67	8.94	7.477	0.840
Pb^{2+}	25	23.69	9.08	7.422	0.898
	35	24.12	9.06	7.429	0.898
	45	24.59	9.04	7.438	0.899
Ni^{2+}	25	11.43	8.54	7.650	0.865
	35	11.86	8.51	7.666	0.863
	45	12.31	8.47	7.683	0.864
Cr(VI)	25	10.55	8.50	7.668	0.882
	35	10.79	10.79	7.678	0.880
	45	11.07	11.07	7.690	0.880
As(V)	25	12.65	8.69	7.587	0.916
	35	13.08	8.65	7.601	0.915
	45	13.52	8.62	7.616	0.914

Table S4
Efficiency of pollutant removal by AS3-PAN from real water sample (pH ~ 6.6)

Wastewater before treatment		Wastewater after treatment	
Ions	mg L^{-1}	mg L^{-1}	Removal %
Pb^{2+}	3.7	1.92	48.11
Fe^{3+}	2.5	1.2	52.00
Al^{3+}	0.1	0	100.00
Ca^{2+}	50	38.4	23.20
Mg^{2+}	18	6.8	62.22
Cd^{2+}	0.02	0	100.00
Ni^{2+}	0.9	0.58	35.56
Zn^{2+}	1.16	0.9	22.55
Cr(VI)	0.07	0	100.00
As(V)	42	22	52.4
SO_4^{2-}	58	53.4	7.93
Cl^-	33	30	9.10

Table S5
Comparison of PAN based adsorbents and amino modified adsorbent for Cd^{2+}, Pb^{2+}, Ni^{2+}, Cr(VI) and As(V) adsorption

Adsorbent	Ion	C_i, mg L^{-1}	q_e, mg g^{-1}	Reference
Macroporous PAN/hydroxyapatite composite	Cd^{2+}	50.0	6.12[a]	[S14]
DR-EDTA[b] modified PAN membranes	Cu^{2+}	20.0	47.6[a]	[S15]
Thio-functionalized PAN fiber	Cd^{2+}	20.0–500.0	368.8[a]	[S16]
PAN/magnetite nanofibers	Pb^{2+}	50.0	156.25[a]	[S17]
Hydrolyzed oxidized PAN nanofibers	Pb^{2+}	100.0	116.2	[S18]
Hydrolyzed oxidized PAN nanofibers	Cd^{2+}	100.0	85.7	[S18]
Hydrolyzed oxidized PAN nanofibers	Ni^{2+}	100.0	21.0	[S18]
Aminated PAN nanofibers	Pb^{2+}	40.0–1,000.0	60.6[a]	[S19]
PAN/organobentonite Composite	Cd^{2+}	10.0–75.0	52.6[a]	[S20]
Iron oxide nanoparticle loaded PAN nanofibers	As(V)	5.0	851.7	[S21]
Amino functionalized PAN fibers	As(V)	50.0–100.0	327.26[a]	[S22]
MoS_2@PANI/PAN nanocomposite[c]	Cr(VI)	2.0	6.57[c]	[S23]
Aminated waste PAN fibers	Pb^{2+}	0.1–10.0	58.94[a]	This work
Aminated waste PAN fibers	Cd^{2+}	0.1–10.0	41.07[a]	
Aminated waste PAN fibers	Ni^{2+}	0.1–10.0	32.15[a]	
Aminated waste PAN fibers	As(V)	0.1–10.0	26.50[a]	
Aminated waste PAN fibers	Cr(VI)	0.1–10.0	24.54[a]	

[a]Determined from Langmuir model.
[b]DR-EDTA - diazoresinethylenediaminetetraacetic acid.
[c]Molybdenum disulfide at hybrid acid-doped polyaniline immobilized on porous polyacrylonitrile nanofiber and q_e, is given in mmol g^{-1}

Table S6
Response surface methodology fitting ANOVA test for the adsorption of Pb^{2+} on AS3-PAN

q	Sum of squares	Degree of freedom	Mean square	Mean	C.V.[a],%
Model	32.30	4	8.08	1.77	44.90
Residual	12.66	20	0.63	–	–
Total	44.96	24	–	–	–

[a]C.V. – coefficient of variation

Table S7
Values from the error data analysis for the adsorption of Pb^{2+} on AS3-PAN

Errors	
HYBRID	183.94
MPSD	148.62
ARS	1.390
ARE	71.26
Std. Error	8.487
COD	0.4968

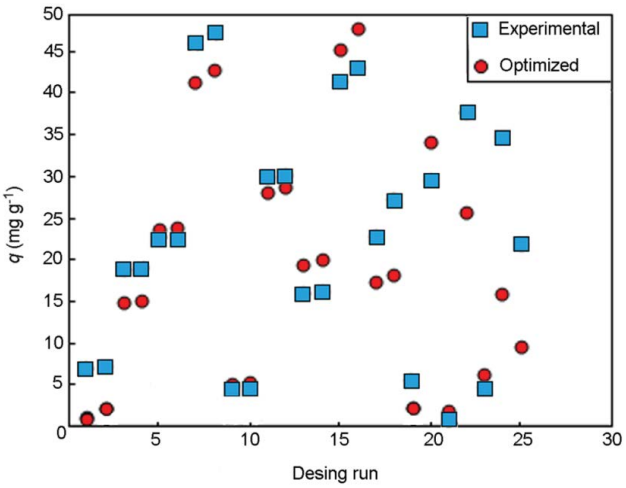

Fig. S5. Experimental and optimized data for the adsorption of Pb^{2+} on AS3-PAN.

S1.7. Desorption study

One of main goal of the design of highly applicable adsorbent is related to minimization of material cost, achievement of high adsorption capacities and long-term adsorbent use. The number of the cycles of adsorbent reuse largely influences techno-economical aspect of an adsorption process. Due to this, newly synthesized adsorbents were subjected to reusability study by variation of process parameters: concentration and regenerator type. Also, the development of efficient desorption technology would help in decreasing of generation of spent adsorbent. This fact will be unavoidably considered in a techno-economic analysis before possible practical applications of developed adsorbents, that is, scale-up of adsorbent synthesis and technology development.

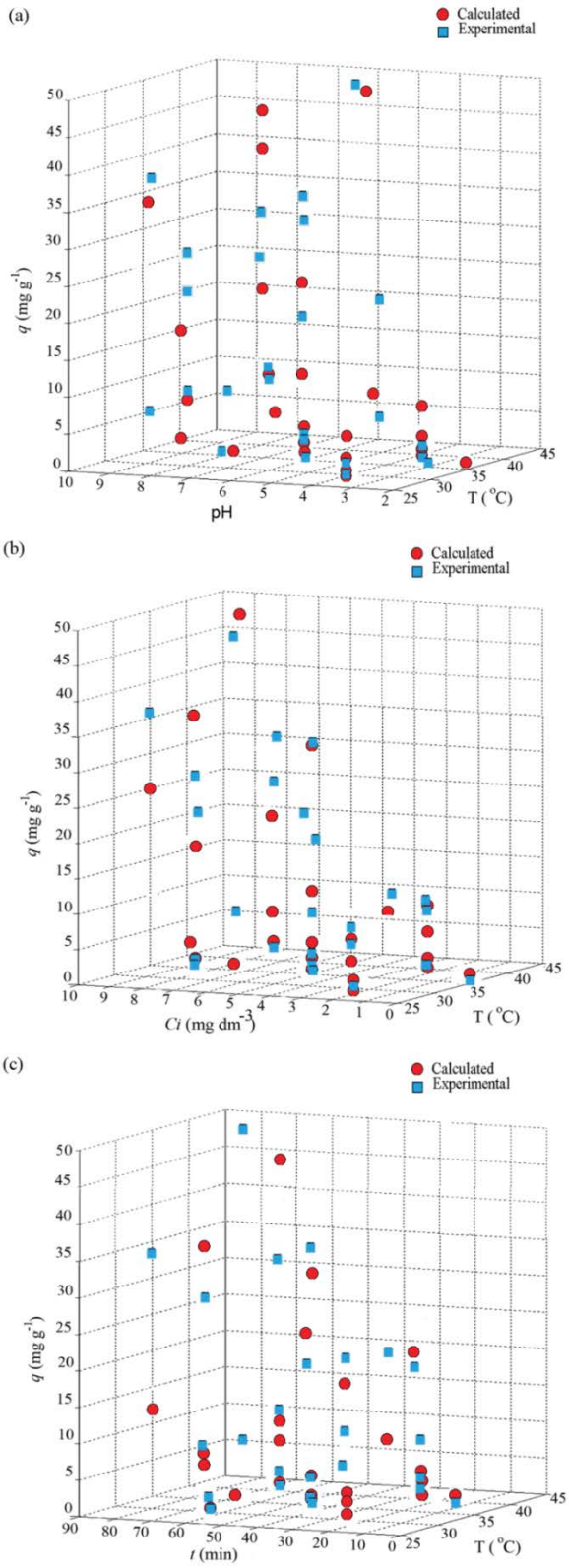

Fig. S6. Correlation between experimental data and design depending on the variable factors, pH value (a), the initial concentration of (b) and the time (c) vs. temperature for the adsorption of Pb^{2+} on AS3-PAN.

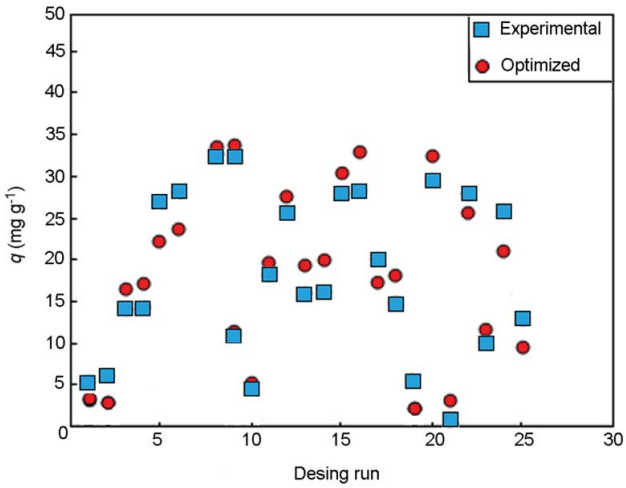

Fig. S7. Experimental and optimized data for the adsorption of Ni^{2+} on AS3-PAN.

S1.8. Effect of interfering ions

Evaluation of AS3-PAN adsorbent for cations/anions removal from real water samples was performed using natural water from the area of the city of Zrenjanin (located in Vojvodina, Serbia). Prior to adsorption oxidation process by air bubbling was performed to provide As(III) and Cr(III) oxidation. Effect of interfering anions showed significant influence on decrease of the efficiency of all studied ions removal (Table S4). Tolerable limit was defined as the highest amount of foreign ions that produced an error not exceeding ±5% in the determination of analyte ions.

S1.9. Comparison of AS3-PAN adsorbent performance with literature data

Collected data from actual literature data on adsorption results related to PAN based adsorbents and amino modified adsorbent for Cd^{2+}, Pb^{2+}, Ni^{2+}, Cr(VI) and As(V) removal are given in Table S5.

S1.10. Prediction of the removal of Cd^{2+}, Pb^{2+} and Ni^{2+} ions using AS3-PAN

ANOVA results indicate that the linear model is significant (F-value = 12.76) with standard deviation of 0.80 and with p-value < 0.0001. The R^2 value of 0.7185 shows that design data were in good agreement with the experimental data. The predicted R^2 value of 0.5681 is in reasonable agreement with the adjusted R^2 value of 0.6622, with a signal to noise ratio of 10.8. All the variables showed significant effect on the output.

Obtained fitting function is presented in the Eq. (S16).

$$\ln(q) = -3.19736 + 0.0068687T + 0.42811\text{pH} + 0.28363C_i + 0.016389t \quad \text{(S16)}$$

The data analysis was realized using Hybrid fractional error function (HYBRID); Marquardt's percent standard

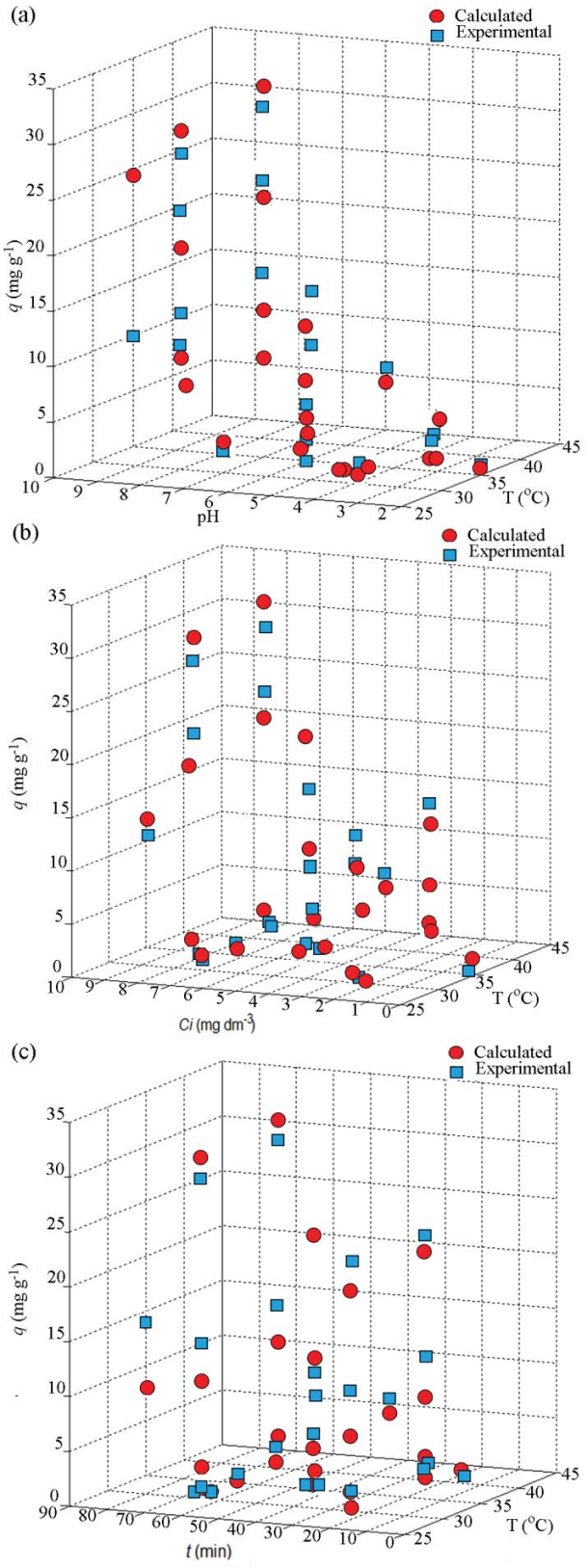

Fig. S8. Correlation between experimental data and design depending on the variable factors, pH value (a), the initial concentration of (b) and the time (c) vs. temperature for the adsorption of Ni^{2+} on AS3-PAN.

deviation (MPSD); Average relative standard error (ARS); Average relative error (ARE); standard error and COD. The Data Analysis Tools Add-in included in the Microsoft's Excel was used to calculate error functions for available data. The error values were given in Table S7.

The correlation between experimental and designed (theoretical) data is shown in Figs. S5 and S6 for Pb^{2+} on AS3-PAN, while Figs S7 and S8 for Ni^{2+} on AS3-PAN.

S1. References

[S1] Z. Veličković, G.D. Vuković, A.D. Marinković, M.S. Moldovan, A.A. Perić-Grujić, P.S. Uskoković, M.D. Ristić, Adsorption of arsenate on iron(III) oxide coated ethylenediamine functionalized multiwall carbon nanotubes, Chem. Eng. J., 181–182 (2012) 174–181.

[S2] G.D. Vuković, A.D. Marinković, S.D. Škapin, M.D. Ristić, R. Aleksić, A.A. Perić-Grujić, P.S. Uskoković, Removal of lead from water by amino modified multi-walled carbon nanotubes, Chem. Eng. J., 173 (2011) 855–865.

[S3] American Society for Testing and Materials, ASTM D1617-07, Standard Test Method for Ester Value of Solvents and Thinners, 2007.

[S4] American Society for Testing and Materials, ASTM D3644, Standard Test Method for Acid Number of Styrene-Maleic Anhydride Resins, 2015.

[S5] S.A. Jafari, S. Cheraghi, M. Mirbakhsh, R. Mirza, A. Maryamabadi, Employing response surface methodology for optimization of mercury bioremediation by vibrio parahaemolyticus PG02 in coastal sediments of bushehr, Iran, CLEAN - Soil Air Water, 43 (2015) 118–126.

[S6] M.M. Haring, The Theory of Rate Processes, J. Chem. Educ., 19 (1942) 249.

[S7] S. Lagergren, About the theory of so-called adsorption of soluble substances, K. Sven. Vetenskapsakademiens, 24 (1898) 1–39.

[S8] Z. Ren, G. Zhang, J.P. Chen, Adsorptive removal of arsenic from water by an iron-zirconium binary oxide adsorbent, J. Colloid Interface Sci., 358 (2011) 230–237.

[S9] M.J.D. Low, Kinetics of chemisorption of gases on solids, Chem. Rev., 60 (1960) 267–312.

[S10] F.-C. Wu, R.-L. Tseng, R.-S. Juang, Characteristics of Elovich equation used for the analysis of adsorption kinetics in dye-chitosan systems, Chem. Eng. J., 150 (2009) 366–373.

[S11] W.J. Weber, J.C. Moris, Kinetics of adsorption on carbon from solution, J. Sanit. Eng. Div., 89 (1963) 31–59.

[S12] D.O. Cooney, Adsorption Design for Wastewater Treatment, Lewis Publishers, Boca Raton, 1999.

[S13] J. Crank, Mathematics of Diffusion, Oxford at the Clarendon Press, London, England, 1956.

[S14] X. Wang, B.G. Miin, W.-S. Lyo, V. Chihaia, M. Gartner, T. Stoica, J.Y. Bae, S.-H. Suh, Column study of cadmium adsorption onto polyacrylonitrile/hydroxyapatite, Rev. Roum. Chim., 55 (2010) 443–447.

[S15] X. Zhang, S. Yang, B. Yu, Q. Tan, X. Zhang, H. Cong, Advanced modified polyacrylonitrile membrane with enhanced adsorption property for heavy metal ions, Sci. Rep., 8 (2018) 1260.

[S16] S. Deng, G. Zhang, S. Liang, P. Wang, Microwave assisted preparation of thio-functionalized polyacrylonitrile fiber for the selective and enhanced adsorption of mercury and cadmium from water, ACS Sustainable Chem. Eng., 5 (2017) 6054–6063.

[S17] H. Malik, U.A. Qureshi, M. Muqeet, R.B. Mahar, F. Ahmed, Z. Khatri, Removal of lead from aqueous solution using polyacrylonitrile/magnetite nanofibers, Environ. Sci. Pollut. Res., 25 (2018) 3557–3564.

[S18] S.H. Lee, Y.G. Jeong, Y.I. Yoon, W.H. Park, Hydrolysis of oxidized polyacrylonitrile nanofibrous webs and selective adsorption of harmful heavy metal ions, Polym. Degrad. Stab., 143 (2017) 207–213.

[S19] P. Kampalanonwat, P. Supaphol, Preparation and adsorption behavior of aminated electrospun polyacrylonitrile nanofiber mats for heavy metal ion removal, ACS Appl. Mater. Interfaces, 2 (2010) 3619–3627.
[S20] T.S. Anirudhan, M. Ramachandran, Synthesis and characterization of amidoximated polyacrylonitrile/organobentonite composite for Cu(II), Zn(II), and Cd(II) adsorption from aqueous solutions and industry wastewaters, Ind. Eng. Chem. Res., 47 (2008) 6175–6184.
[S21] D. Morillo, M. Faccini, D. Amantia, G. Pérez, M.A. García, M. Valiente, L. Aubouy, Superparamagnetic iron oxide nanoparticle-loaded polyacrylonitrile nanofibers with enhanced arsenate removal performance, Environ. Sci. Nano, 3 (2016) 1165–1173.
[S22] H. Deng, K. Li, Efficient removal of arsenate by a surface functionalized chelating fiber based on polyacrylonitrile, Environ. Prog. Sustainable Energy, 35 (2016) 1634–1641.
[S23] J. Qiu, F. Liu, S. Cheng, L. Zong, C. Zhu, C. Ling, A. Li, Recyclable nanocomposite of flowerlike MoS_2@hybrid acid-doped PANI immobilized on porous PAN nanofibers for the efficient removal of Cr(VI), ACS Sustainable Chem. Eng., 6 (2018) 447–456.